20

Inelastic lepto-production in the Lund model, the soft radiation model and the linked dipole chain model

20.1 Introduction

As usual in connection with the Lund model we will start with a semi-classical string scenario to describe a deep inelastic scattering (DIS) event. We will show that if the target is a meson state of the yoyo type then the final state obtained, after a large momentum transfer to one of the endpoints q_0 or $\bar{q}_0$, is very similar to the state obtained in an e^+e^- annihilation event as long as we neglect gluon emission.

Depending upon the Lorentz frame used to describe the string motion, we obtain different shapes of the final state. If we use the final-state cms frame we obtain a longitudinally stretched string, which, if it does not break up, will have a length $\simeq W/\kappa$ just like the flat e^+e^- annihilation $q_0\bar{q}_0$-strings of the same cms energy W. This time the state will, however, contain a small bend. But the transverse extension of the state is always of order m/κ, with m the original meson mass. Therefore the transverse dimensions are in general negligible compared to the longitudinal size.

We will show that the properties related to the breakup of such a string state only depend upon *projections onto the momentum transfer direction.* Therefore it is easy to generalise the Lund model fragmentation formulas to such final states.

After that we consider a corresponding model for DIS from a baryon. We will use a simple but nontrivial string model for the baryon. We show that even if the baryon is not a yoyo string state, the final-state string will nevertheless look very similar to a stretched-out yoyo, almost independently of how it is hit.

This will also lead us to some considerations of baryon fragmentation. We will show how the baryon number is conserved in the Lund model breakup process. We note, however, that there are many question marks

https://doi.org/10.1017/9781009401296.020 Published online by Cambridge University Press

in connection with baryon fragmentation, partly because there are so few experimental data available at present.

Then we discuss the way in which the Lund model treats situations when the momentum transfer Q^2 acts on an ocean quark or antiquark. This is a part of the cross section which is expected to grow fast with the energy and therefore it will be more and more important for the future.

In the original Lund treatment as it is implemented in the Monte Carlo simulation program LEPTO, [63], the final state is treated as a two-string situation with a rather *ad hoc* parametrisation of the energy sharing between the three original valence quarks and the left-over ocean q ($\bar{q}$), if it is the ocean $\bar{q}$ (q) that is struck.

It is possible to make a case for a more precise structure from considerations of the time development of the final state, at least if the ocean partons are intrinsic parts of the wave function of the hadron. We present these ideas as they are implemented in the Monte Carlo program ARIADNE, [92].

Next we go over to gluon radiation for a DIS event in the Lund model. We introduce a model, the soft radiation model (SRM), [11], of a different kind from the one we considered in the last chapter in the context of the conventional ISB scenario.

The basic ideas are the following. Even if the final state in a DIS event develops on a long time scale in a way similar to the corresponding state in an e^+e^- annihilation event, there is one major difference on the short time scale relevant to gluon emission. In e^+e^- annihilation the produced q_0 and $\bar{q}_0$ are both expected to be essentially pointlike. This means that all the energy is readily available for gluon emission when they start to separate, forming the original dipole.

In DIS events, the struck-out parton is expected to be pointlike in the same sense. If it is a q_0, i.e. a color-3, *there is no reason why the corresponding color-*$\bar{3}$ *charge should be localised in the same way.* It is, in fact, probably spread out over all the remainder state. Similarly, while the struck parton's energy-momentum after the collision, in the notation of the last chapter Q_-, is strongly concentrated, the hadron remainder will contain the total energy-momentum $P_+ - Q_+$ in a (space-)extended form.

This means that the radiation in this case occurs from something similar to an extended 'antenna source'. It is well known that coherent emission of wavelengths much smaller than the antenna size is strongly suppressed. We have already discussed the notion of a *form factor* to describe extended charge distributions, cf. the size parameter in Eq. (5.47). For a wavelength larger than this size there is no difference between a pointlike and an extended charge. But for a smaller wavelength, corresponding to momentum transfers larger than e.g. the parameter $M_0 \simeq 0.7$ GeV

https://doi.org/10.1017/9781009401296.020 Published online by Cambridge University Press

in the elastic baryon form factors of Eq. (5.47), there is power suppression.

The SRM suggests one possible method to treat the extension. It contains two basic parameters, which have been investigated using the experimental data available at present. One of the parameters, corresponding to the inverse of the transverse size of a hadron, turns out from the experimental data to be of the order 0.5–1 GeV. The other parameter corresponds to the (space) dimensions of the extended system and for it we obtain in a very stable way the number 1. This would evidently be typical of a string or, remembering a motivation for the string presented in Chapter 6, of a vortex-line force field.

Since the SRM was suggested several years ago, [11], based upon arguments like those presented above, it is quite surprising that its implications are similar to those obtained from the CCMF model, [44], cf. Section 19.6. We will show that the so-called non-local form factor in that approach actually on average cuts off the gluon radiation along the same lines in phase space as the SRM.

After that we will introduce a different approach, which is very natural within the Lund model, where *all QCD properties are treated in accordance with dipole properties.* The Lund dipole cascade model describes the partonic states in timelike cascades (occurring in particular in e^+e^- annihilation events) in terms of the decay of color dipoles, as discussed in Chapters 16–18. Then the fragmentation process converts the ensuing string states into 'ultimate dipoles', i.e. hadrons modelled by means of $q\bar{q}$-states, with the charges stemming from different vertices connected by string-field pieces.

In section 20.7 we will show that if one probes such a hadronic dipole entity then the virtual states, i.e. the states encountered by a short-time probe, can also be most easily described in terms of dipoles, in particular in terms of *chains of linked dipoles.* To be more precise we will show that the CCMF model described in section 19.6 can be generalised and simplified into such a statement. As this is a very recent result, [16], within the Lund Group we will be content to describe the general ideas incorporated in the *linked dipole chain model* (LDC) and only briefly consider the consequences (in particular with respect to the ongoing measurements in HERA).

20.2 The classical motion of a yoyo-string exposed to a large momentum transfer at an endpoint

We start by considering the motion of a yoyo-hadron the constituents of which are originally moving in and out, as shown in Fig. 20.1 in the lab frame, in which the state is at rest before the momentum transfer. We have

https://doi.org/10.1017/9781009401296.020 Published online by Cambridge University Press

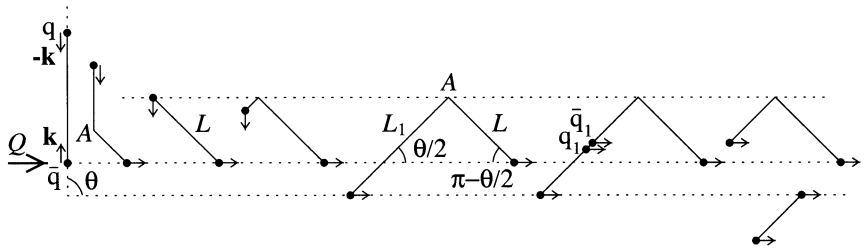

Fig. 20.1. The development of a yoyo-state, originally at rest, after a large momentum transfer. The notation is explained in the text.

already discussed string motion in detail several times and will therefore be brief.

The two endpoint particles will have momenta $\pm\mathbf{k}$ along the string direction at the beginning. The main phases in the development after the string is hit at an endpoint with a momentum transfer $\mathbf{Q}$ are as follows.

- Suppose that the endpoint $\bar{q} \equiv \bar{q}_0$ is struck and moves along the direction $\mathbf{Q} + \mathbf{k}$ (at an angle θ with respect to the original string direction) with constantly decreasing energy-momentum. Its partner at the opposite endpoint, q_0, is as yet unaware of this and moves downwards gaining energy-momentum from the string.

- A straight string section L (with angle $(\pi - \theta)/2$ with respect to the string) is formed and a disturbance 'corner' A moves along the string (but does not carry any energy-momentum). The transverse velocity of L is $v_\perp = \cos(\theta/2)$ since the corner and $\bar{q}_0$ move with the velocity of light.

- The q_0 meets the corner A. The string is 'soft' and affects q_0 only with the finite force κ so that q_0 just continues downwards. A new segment L_1 is formed while the q_0 is losing energy, until it stops (at the same point where it would have stopped if there had been no momentum transfer to $\bar{q}_0$). The transverse velocity of L_1 is $v_{\perp 1} = \sin(\theta/2)$.

- The q_0 is then dragged along by the string and it will move along a line parallel to $\mathbf{Q} + \mathbf{k}$. If we boost to a system in which L_1 is at rest then q_0 actually moves along the string segment. In the lab frame the angle between the string segments L and L_1 is always $\pi/2$.

- From now on the string segments L and L_1 both serve as 'transporters' of energy-momentum from $\bar{q}_0$ to q_0.

https://doi.org/10.1017/9781009401296.020 Published online by Cambridge University Press

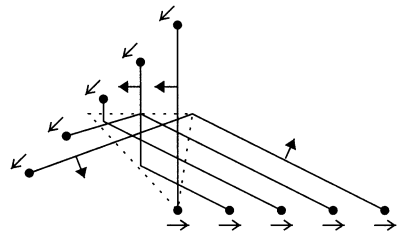

Fig. 20.2. The development of a yoyo-state exposed to a large momentum transfer, shown in the final-state cms.

We also show in Fig. 20.1 a breakup of the string; its characteristics will be discussed further below. But before this the string state looks like a rigid body moving forward in a triangular shape along the $(\mathbf{Q}+\mathbf{k})$-direction. In the lab frame the state evidently has an extension of the same order both transversely and longitudinally with respect to the momentum transfer. However, the state is moving very fast longitudinally if the momentum transfer is large.

The total momentum is evidently $\mathbf{Q}$ and the total energy is $|\mathbf{Q}+\mathbf{k}|+M-|\mathbf{k}| \simeq |\mathbf{Q}|+M-|\mathbf{k}|(1-\cos\theta)$, where we have developed the square root $|\mathbf{Q}+\mathbf{k}|$ as $\sqrt{Q^2+k^2+2\mathbf{k}\cdot\mathbf{Q}}$ to lowest order in $|\mathbf{k}|$. We conclude that the velocity is $\simeq 1-[M-2|\mathbf{k}|\sin^2(\theta/2)]/Q$.

It is also useful to consider the state in the cms after the momentum transfer, i.e. in this frame the struck $\bar{q}_0$ will move away with the cms energy $W/2$ along the $(\mathbf{Q}+\mathbf{k})$-direction and the remainder state will move as a whole with energy $W/2$ in the opposite direction. An approximate formula for W is $W \simeq \sqrt{2Q[M-2|\mathbf{k}|\sin^2(\theta/2)]}$, which is easy to derive from the results in the last paragraph.

This situation is shown, for simplicity for the choice $\theta=\pi$, in Fig. 20.2 and we leave it to the reader to go through the development. The most noticeable thing in this case is that the state has become much longer longitudinally, i.e. if it does not break it will now be of order W/κ, while it is still of order m/κ transversely.

The lab-frame size is evidently an effect of Lorentz contraction, cf. Chapter 2. In the cms frame the bend around the corner is hardly noticeable and the situation is very similar to the flat e^+e^- annihilation $q\bar{q}$-strings we have treated before.

https://doi.org/10.1017/9781009401296.020 Published online by Cambridge University Press

20.3 The fragmentation of a final-state yoyo-string stemming from a DIS event

We start by noticing that the two string segments L and L_1 in Fig. 20.1 both carry energy and momentum because they are moving. Thus a small element, dl, along L_1 will have, in the lab frame, energy dE and momentum $d\mathbf{p}$, with components dp_ℓ along the direction $\mathbf{Q}+\mathbf{k}$ and $dp_\perp$ transverse to it:

$$dE = \frac{\kappa dl}{\cos(\theta/2)}, \quad dp_\perp = \kappa dl \, \sin(\theta/2), \quad dp_l = \kappa dl \tan(\theta/2)\sin(\theta/2) \tag{20.1}$$

If the string breaks up into small parts then all of these, besides one, will be plain yoyo-states. The exception is the part containing the bend. Just as in connection with the breakup of strings with internal excitation gluons, cf. Chapter 15, we assume that the occurrence of such a bend still allows the same projection onto the hadronic states of a given mass.

We will next show that all properties related to the decay of the string depend only upon the longitudinal projections along $\mathbf{Q}+\mathbf{k}$. We start by considering the production of a $q_1\bar{q}_1$-pair along the segment L_1 in accordance with Fig. 20.1.

It is easy to convince oneself that, if the q_1 and $\bar{q}_1$ start out as massless and without energy, the $\bar{q}_1$ will move along the dotted line and together with the q_0 will form a yoyo-state. To prove this note that in the rest frame of the string piece L_1 the q_1 and $\bar{q}_1$ will move along the string with the velocity of light in opposite directions. Therefore in the frame where L_1 moves with the transverse velocity $\sin(\theta/2)$ they will both move at an angle $\theta/2$ with respect to the L_1-direction.

If we assume that the break occurs at a distance δ from the q_0 then we may calculate the following energy-momentum fraction,

$$z_- = \frac{E - p_\ell}{(E - p_\ell)_{tot}} \tag{20.2}$$

for the string piece. The variable z_- is Lorentz-invariant and it is the relevant variable in the target fragmentation region. For large energies it coincides with the Feynman scaling variable x_F, which is often used in hadronic collisions.

We note that $(E-p_\ell)_{tot}$ corresponds to the total longitudinal size of the system and that for the system $(\bar{q}_1, \delta, q_0)$ we have

$$E - p_\ell = \kappa\delta\cos(\theta/2) = \kappa\delta_\ell \tag{20.3}$$

according to the formulas derived above. Note that the energy-momentum of the $\bar{q}_0$ does not occur in the difference. This means that the variable

https://doi.org/10.1017/9781009401296.020 Published online by Cambridge University Press

z_- only depends upon the longitudinal projection, $\delta_\ell = \delta \cos(\theta/2)$, of the string size. Further, the remainder system after the $q_1\bar{q}_1$-break will move as a rigid triangle with a final-state mass $M_1^2 \simeq (1 - z_-)W^2$, which again only depends upon the longitudinal projection.

Finally, if the production probability per unit time for a $q\bar{q}$-pair is proportional to the tension in the rest system of the relevant string piece then, owing to time dilation, it will be proportional to $\sqrt{1 - \mathbf{v}_\perp^2}$ in a frame where the string piece moves with transverse velocity $\mathbf{v}_\perp$, as was shown in Chapter 15:

$$\mathcal{T} = \kappa\sqrt{1 - \mathbf{v}_\perp^2} \tag{20.4}$$

In this way the probability of producing a pair in the string element $d\sigma$ in L_1 is again proportional to the longitudinal projection:

$$d\sigma\sqrt{1 - \mathbf{v}_\perp^2} = d\sigma \cos(\theta/2) = d\sigma_\ell \tag{20.5}$$

If, however, we consider the breakup properties in the segment L we find a corresponding factor $(\sqrt{1 - \mathbf{v}_\perp^2})_L = \sin(\theta/2)$. This will be the longitudinal projection factor for all elements of L. In this case the relevant fragmentation variable is z_+ and we note that we will have the relation

$$z_+ z_- = \frac{m_\perp^2}{W^2} \tag{20.6}$$

Thus for particles with large z_+ we will have tiny z_- components, corresponding to (seemingly) small longitudinal string elements.

We conclude that Lund model fragmentation can be performed just as for an e^+e^- annihilation event and that the process is Lorentz-invariant if we use the longitudinal projections of the string state. In this case there is also some intrinsic transverse momentum, which stems from the original motion of the q_0 and the $\bar{q}_0$ before the momentum transfer. We note that the transverse momentum component of the $\bar{q}_0$, $\mathbf{k}$, is carried forward to the so-called *quark fragmentation region* or *current fragmentation region*, while the component carried by the q_0, $-\mathbf{k}$, will be subdivided among the final-state particles in the target fragmentation region.

This means that there is a long-range compensation (i.e. the compensation occurs in regions with large relative rapidity) of this transverse momentum. This original motion is usually termed the *Fermi motion* inside the hadronic state (in accordance with the nomenclature for the motion of the nucleons in a bound nucleus). It turns out, however, that this effect is hardly noticeable at large values of Q, compared to the noise stemming from the gluon emission.

https://doi.org/10.1017/9781009401296.020 Published online by Cambridge University Press

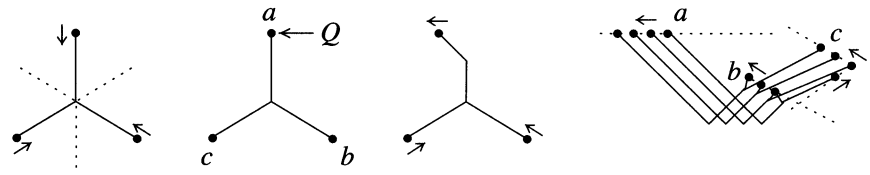

Fig. 20.3. A simple string model for a baryon and the way the state responds to a large momentum transfer.

20.4 A model for baryon fragmentation

1 A valence, i.e. endpoint, q is struck

In order to obtain a nontrivial model for an initial baryon state we assume that the three q-particles are all connected via strings to a common point, which we will call the *junction*, in accordance with Fig. 20.3. The junction does not carry any energy-momentum. It is merely a device which moves in such a way that the total tension at rest for the three connected string pieces will vanish, i.e. the strings are in equilibrium.

The baryon model has in the same way as the yoyo-states the property that, in the mean, half the energy will be kinetic energy of the q-particles while the other half is potential energy in the string's constituent gluons. We consider the motion of this state when one of the q's, called a in the figure, is struck thereby undergoing a large momentum transfer. The other two are denoted b and c and the direction along the momentum transfer is $\mathbf{n}$.

When a moves away along $\mathbf{n}$ there will be a bend on the adjoining a-string, which will move inwards towards the junction. Assuming that at the start of the motion all three q's are moving inwards, the bend will reach the junction at the same time as b and c arrive. After this the junction will start to move with a velocity determined by $\mathbf{n}$, i.e. the a-direction of motion. The reason is that in the rest frame of the junction there must always be an angle $2\pi/3$ between the three string pieces.

We will not trace the rest of the motion in detail but we note that both b and c will continue to move towards the places where they would have stopped if there had been no momentum transfer. Only after that will they start to respond to the momentum transfer and move after a. This is due to causality, i.e. that there is a finite transmission velocity of information along the force field.

It is a remarkable fact that, in almost all cases, in whichever direction $\mathbf{n}$ we hit a, roughly speaking one of b or c will go in the opposite direction

https://doi.org/10.1017/9781009401296.020 Published online by Cambridge University Press

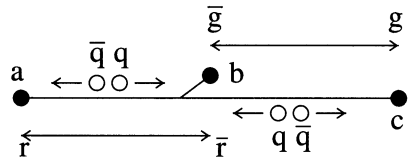

Fig. 20.4. The general appearance of a baryon which has been exposed to a large momentum transfer. The colors are exhibited together with the color fields between the forward quark a and the two backwards quarks (b and c) with the field $r\bar{r}$ and similarly between a, b and c with the field $\bar{g}g$. The drag force on produced pairs in the two segments is also exhibited.

while the other will go along **n**. This means as shown in Fig. 20.3 that b will end up with a rather short piece of string connecting it to the junction, while c will move away and end up far back before it is turned around. The size of the string segment around b will in practice serve as a kind of effective mass for b. The parton b will move repeatedly up and down around the junction but the effective mass will always be a rather small fraction of the original baryon mass.

The emerging picture is then of an essentially longitudinally stretched object with one of the valence q's moving out along the momentum transfer, the second moving initially away and the third staying in the middle. A simplified version of such a state is shown in Fig. 20.4, and from this picture we may deduce a consistent way to treat the fragmentation in the Lund model.

We note that the whole state is a color singlet and consequently if a is colored r, b colored b and c colored g we will have at the forward end a color-3, r, joining a color-$\bar{3}$, composed of $\mathrm{bg} = \bar{\mathrm{r}}$ at the backward end. Similarly the segment between c and the forward-moving parts will behave like a $\bar{\mathrm{g}}\mathrm{g}$-string.

This means that if the string breaks up between a and b then the $\bar{q}$ from the break will be dragged towards a, and the q towards the color-$\bar{3}$ bc. Similarly, a break in the backward-moving string part will cause the $\bar{q}$ to move towards c and the q to move towards ab. In this way *there will always be a baryon produced around the junction*, while the rest fragments like ordinary Lund string pieces, including baryon-antibaryon production (possible at least in the high-energy forward part).

It is possible to make many further semi-classical remarks, [8], based upon this simple model. We will be content to say that there is no really well understood picture for the fragmentation of a baryon. Within the JETSET Monte Carlo scenario there are several phenomenologically

https://doi.org/10.1017/9781009401296.020 Published online by Cambridge University Press

reasonable predictions, which, owing to the small amount of data, are rather little tested in the present DIS experiments.

The JETSET Monte Carlo implements the structure we have introduced in the popcorn model for baryon-antibaryon production in Chapter 13. To that end we assume that target fragmentation will act just as in the $B\bar{B}$ production case after a $\bar{B}$ has already been produced. Then there is a given probability that the first-rank hadron is a particular baryon or that it is a particular meson and the baryon is then the second-rank particle. Then the remainder of the state is treated as an ordinary $q\bar{q}$-string fragmentation event.

2 *An ocean q or $\bar{q}$ is struck*

There is one kind of event upon which we have not touched as of yet, although it corresponds to a large cross section in DIS and the cross section grows with the energy. In these events an ocean quark or antiquark is struck, in contrast to the situation we have discussed above when we have always struck a valence q or $\bar{q}$, an endpoint of the string.

Here the target region will contain either three valence q's and one ocean q (if it is the ocean $\bar{q} \equiv \bar{q}_o$ that is struck) or else there will be three valence q's and an ocean $\bar{q}$ left (the ocean $q \equiv q_o$ is struck). We will call these situations cases A and B, respectively. There is no straightforward unique way to treat them dynamically and within the Lund model there have been two different suggestions, one which is used in the LEPTO Monte Carlo, [63], and one in ARIADNE, [10].

In the LEPTO treatment the final state contains the fragmentation of two distinct strings. For case A there will be a small baryonic string, between the ocean q_o and two of the valence q's, and a large mesonic one between the remaining valence q and the struck ocean $\bar{q}_o$. For case B there will be the opposite situation with the struck ocean q_o joined to a large baryonic string with two valence q's and the remaining valence q joined to a small mesonic string with the remaining ocean $\bar{q}_o$. 'Large' and 'small' here describe the energies and masses of the strings. There is a rather *ad hoc* parametrisation of the energy sharing: the treatment is only meant to provide a possible parametrisation of data.

It is possible to be a bit more sophisticated and to introduce somewhat more structure, based upon the expected time development of the state. The ocean components of the structure functions must be considered as long-lived parts of the fluctuations. Such parts, which we have discussed within the conventional ISB scenario in Chapter 19, stem from the DGLAP evolution equations. They are usually called 'intrinsic'.

There is also a possibility, which can be calculated in perturbation theory, that the process proceeds through the channel $\gamma^* g \to \gamma^*(q\bar{q})$ (usually

https://doi.org/10.1017/9781009401296.020 Published online by Cambridge University Press

named *boson-gluon fusion*). Then the lepto-production probe interacts with the short-lived fluctuation of an intrinsic gluon into a $q\bar{q}$-pair. It is difficult to distinguish between the two situations because the DGLAP mechanism stems from the same perturbative contribution.

In perturbation theory it is always the main momentum transfer behaviour which decides whether one diagrammatic contribution will dominate over other possible contributions. Later in this chapter, in connection with the linked dipole chain model, we will exhibit this feature in much more detail. For the present we make the following reasonable partitioning.

An intrinsic component in the hadron wave function ought to 'thermalise' in the sense that the ocean q_o and $\bar{q}_o$ should no longer be directly connected. If the interaction picks up an ocean q_o then we expect that the (anti-)color charge of its partner is distributed within the hadronic radius. Therefore there should be few (color-dynamical) differences between case B and the case when a valence quark is struck. In both cases the target is effectively in a color-$\bar{3}$ state.

There is nevertheless the difference that there are extra flavor numbers in the target region. In accordance with Lund model ideas we expect that when the struck q_o moves away the vacuum will compress the color field into a thin vortex-like string. When sufficient energy is stored in the field it will break up but this cannot occur until the string (in the rest system of the produced hadron) is larger than a hadronic radius.

This kind of out-moving string should be little affected by the finer details of the target charge distribution and we will therefore assume in accordance with the ARIADNE ansatz, [10], that *the momentum distributions of the final-state hadrons are the ordinary ones encountered in the Lund model.* Thus in the ocean-quark situation we will use the same breakup probabilities as before. We treat case A as in Fig. 20.5(a), i.e. we first produce a baryon at the end containing the q_o and two valence quarks and let the remaining energy go into a final string state between the struck $\bar{q}_o$ and the remaining valence q. Similarly, for case B, shown in Fig. 20.5(b), we choose to produce first a meson between the $\bar{q}_o$ and one valence q; the remaining energy-momentum then goes into a final string between the remaining valence constituents and the struck q_o.

The difference from the LEPTO case is that now there is no a priori energy sharing. The endpoint particle will have the same spectrum as if it were produced as the endpoint particle in any Lund string. Thus the whole momentum transfer is taken by the struck ocean component and we peel off one hadron at the backward end in a stochastical way, thereby defining the energy-momentum of the final remaining string.

In practice when one builds a Monte Carlo simulation it is necessary to include all possibilities. Therefore given a cross section for DIS events

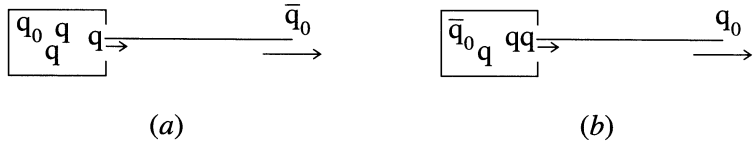

(*a*) (*b*)

Fig. 20.5. The string breakup in the target fragmentation region when the momentum transfer acts on an ocean component that moves away leaving a state which is dragged apart, a particle being produced behind it. The cases (*a*) and (*b*) are explained in the text.

in accordance with Chapters 5 and 19 it is possible to subdivide it into the valence and the ocean parts. There is also the possibility of having a $\gamma^* g$ event (the boson-gluon-fusion (BGF) events described above) and then we use the energy-momentum partitioning prescribed by the perturbative expressions. In order not to double-count the contributions, we require in the BGF case that *the squared energy-momentum transfer between the* q_o *and the* $\bar{q}_o$, $q^2_{\perp n}$, *should be larger than* Q^2. If $q^2_{\perp n} < Q^2$ then the contribution is already included in the conventional structure function cross section, i.e. we have the intrinsic ocean contributions mentioned above.

20.5 The soft radiation model

1 Preliminaries

We start by considering a simple model of DIS from a state with two charged particles bound together as in positronium, see Fig. 20.6. In this figure the state is assumed to move very fast and we also assume that the momentum transfer acts on the e^-. There are then two different but dynamically equivalent ways to look at the situation if we assume that the state is *loosely bound.*

P1 We may say that the e^+ is completely unaffected by the momentum transfer and therefore does not radiate at all. Then all the radiation stems from the e^--current, which comes in and is suddenly changed.

P2 We may alternatively say that there is no radiation from a bound state and therefore all the radiation stems from the dipole which is produced between the e^+ and e^- when the momentum transfer strikes.

https://doi.org/10.1017/9781009401296.020 Published online by Cambridge University Press

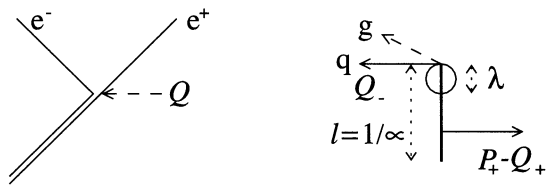

Fig. 20.6. The situation when a loosely bound system is affected by a large momentum transfer (left-hand part) together with the kinematics for the SRM (right-hand part).

We remember from the considerations on the bremsstrahlung cross section in Chapter 16 that these two descriptions will give the same result. They correspond to adding the two diagrams in Fig. 16.1 for case P1 and those in Fig. 16.2 for case P2. The sum of the two diagrams is in both cases gauge-invariant and also provides the same total radiation.

The situation is much more difficult to disentangle if we consider a *strongly bound system.* In that case both the e^+ and e^- are accelerated in the bound system throughout, but in accordance with quantum mechanics there is no radiation as long as the system is in its ground state before the interaction. For the case P1 it is necessary not only to describe the way e^- is localised in the wave function, i.e. to describe the transition from the bound state to a free e^- with a precise value of its energy-momentum. It is also necessary to describe what happens to the remainder system, in particular to the other charge(s), here e^+.

The basic proposal in the soft radiation model (SRM) is that the situation may be more easily described by case P2. This is in particular plausible for QCD because then the field itself is also color charged, so that there may be many charges accelerated during the interaction. We note that in the ordered dipole chains of the dipole cascade model, which directly mirrors the Lund string, these accelerations already occur in a coherent way.

It is also the case that the force field of a bound state has the energy distributed over a region, which for a vortex line or string would be one-dimensional. Any emission would only involve a part of the system and the ordinary radiation conditions mean a size of the order of a fraction of the wavelength. Therefore only that part of the energy-momentum is available for the emission.

In summary, in e^+e^- annihilation reactions the emitters can be considered as essentially pointlike objects but this may no longer be the case for DIS events. The probe, i.e. the field pulse, is well defined in size but the target hadron is extended.

https://doi.org/10.1017/9781009401296.020 Published online by Cambridge University Press

2 The details of the model

If a q-parton, for example, is affected by a momentum transfer such that it obtains a lightcone energy-momentum Q_- then the rest of the state contains the corresponding energy, $P_+ - Q_+$, and the color-$\bar{3}$. Thus the initial dipole contains one pointlike object and one that is extended, in particular with respect to the carrying of energy-momentum (see the right-hand part of Fig. 20.6).

Then a gluon emitted from the phase-space element $(k_\perp, y)$ will need both a positive and a negative energy-momentum lightcone component:

$$k_\pm = k_\perp \exp(\pm y) \tag{20.7}$$

While the negative lightcone component is easily available from the large energy concentration in the struck parton, the positive one is spread over some region. It is a well-known property that coherent radiation of wavelength λ from an emitter of size l, where $\lambda \ll l$, stems only from a fraction of the emitter comparable to λ (shown as a 'bubble' in Fig. 20.6).

Then for a large-$k_\perp$ gluon (which has a small $\lambda \sim 1/k_\perp$) the total positive lightcone component will stem from a fraction of the emitter P_{+r} (the index r stands for the remainder after the struck parton leaves). This means that there will be strong damping of the radiation in the forward direction, i.e. in the target region.

In the SRM it is assumed that the phase-space limits are changed into

$$\begin{aligned} k_+ &< \left(\frac{\mu}{k_\perp}\right)^d P_{+r} \\ k_- &< Q_- \end{aligned} \tag{20.8}$$

where the parameter μ corresponds to the inverse size and d is a number describing the dimensionality of the source-remnant.

The data from the EMC collaboration prefer a value of $\mu \approx 0.6$ GeV/c and $d \approx 1$, according to [11]. This corresponds to a mean transverse extension $\sim \pi/\mu \approx 1$ fm and an essentially one-dimensional energy density as in a string. The data covers a rather small (Q^2, x) range but we will nevertheless, perhaps rashly, assume that the result is valid for all available energies.

We will make one adjustment, however. In the case when there is a large x-interaction the remnant only contains energy-momentum $P_{+r} = (1 - x_B)P_+$, which is less than that of the incoming hadronic state P_+. Assuming that it is *the energy density in the rest system that is constant* we are lead to expect that the effective emitter size l is correspondingly smaller and thus that μ behaves as

$$\mu \equiv \mu(x) = \frac{\mu_0}{1 - x} \tag{20.9}$$

https://doi.org/10.1017/9781009401296.020 Published online by Cambridge University Press

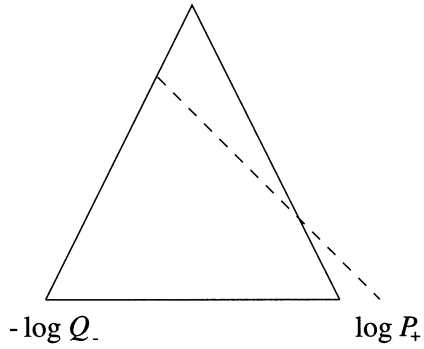

Fig. 20.7. The available phase space for gluon emission in the SRM shown in the κy-plane, where $\kappa = \log k_\perp^2$, with the region above the broken line forbidden (or exponentially suppressed) as described in the text.

This will mean that *the radiation in the target fragmentation region is the same, independently of the interaction*, i.e. the damping is governed by $(\mu_0/k_\perp)P_+$, independently of x and Q^2. The available energy will, however, only permit an emission if the energy-momentum component of the emitted gluon, k_+, is smaller than the available $P_{+r} = (1-x)P_+$.

The allowed emission region in the triangular phase space of the dipole is in this way changed (sometimes very much) in the target fragmentation region of a DIS event (cf. Fig. 20.7). From Eqs. (20.8), (20.9) we conclude that the new phase-space boundaries are

$$\log\left(\frac{k_\perp}{Q_-}\right) < y < \min\left[\log\left(\frac{\mu_0 P_+}{k_\perp^2}\right),\ \log\left(\frac{P_{+r}}{k_\perp}\right)\right] \qquad (20.10)$$

Note that these curves correspond to straight lines in the κy-plane. The damping is, in the present case, of a step function character. If there were to be power suppression in the transverse momentum, as in a form factor, this would correspond to an exponential damping in the κ-variable. The results of the model are, however, rather insensitive to the possibility of such an exponential tail.

20.6 The relationship between the SRM and the non-local form factor of the CCMF model

In the CCMF model Marchesini *et al.*, [44], have used a very general technique to re-sum higher-order perturbative contributions to the basic

https://doi.org/10.1017/9781009401296.020 Published online by Cambridge University Press

ladder diagrams in QCD, in order to obtain the changes in the structure functions for small values of x_B and medium-to-large values of Q^2.

We have described their results in Section 19.6. In the CCMF model one follows an emission line along the fan diagrams, see Fig. 19.1 and there are gluon splittings into z (the main line) and $1-z$ (the ladder gluons). It is implicitly assumed that the pole character of the splitting function implies $z \simeq 0$, i.e. a fast degrading of the energy-momentum fraction along the main line.

Therefore the initial-state bremsstrahlung (ISB) emissions result in a stochastical process of a step-like character in $\log(1/z)$: the next gluon emission is, according to the rules of the model, forced to be behind (i.e. in the dipole phase-space triangle to the left of) the line xP_+ where $x = \prod z_j$ from the previous emissions. Marchesini *et al.* have calculated the virtual corrections to these emissions and obtain a form factor, called non-eikonal, in the weights for producing such states. We have shown in section 19.6 that the non-eikonal form factor actually has the same properties as an 'ordinary' Sudakov factor, i.e. it corresponds to the negative exponential of the regions in which there is no emission, owing to the CCMF choice of ISB gluons. We will now show that *the average boundary of the area forbidden by CCMF is equal to the simple suggestion obtained from the SRM.*

We will thus assume that there is a set of steps in $\log(1/z)$, each one bringing the later emissions backwards a distance $l_j = \log(1/z_j)$. The emitted gluon j also contains transverse momentum, $\mathbf{p}_{\perp j}$, and the main line, i.e. the 'virtual propagator' line, then obtains a recoil $\mathbf{q}_{\perp n} = -\sum^n \mathbf{p}_{\perp j}$. We start with the case when the $p_\perp$'s are ordered such that $p_{\perp 1} \ll p_{\perp 2}$ etc. which also means (in the leading-log approximation) that $\mathbf{q}_{\perp n} \simeq -\mathbf{p}_{\perp n}$. Afterwards we will consider what happens if there is a different ordering (as the Lipatov approach allows, cf. Section 19.5).

In order to move, as we have decided, backwards and upwards in the phase-space triangle we will have to sum over all possibilities to reach the point $l = \sum_{j=1}^n l_j, h = \sum_{j=1}^n h_j$, with

$$h_j = \log(p_{\perp j}^2 / p_{\perp j-1}^2) \tag{20.11}$$

We note that all transverse momenta are in accordance with the case T1 in Section 19.6 and we therefore use the relevant shape of the non-eikonal form factor, i.e. $\exp[-\bar{\alpha}\log^2(1/z_j]$ with $\bar{\alpha} = 3\alpha_s/\pi$, to obtain

$$N(l,h) = \sum \int \prod \bar{\alpha} dl_j dh_j \exp(-\bar{\alpha} l_j^2) \delta\left(\sum l_j - l\right) \delta\left(\sum h_j - h\right) \tag{20.12}$$

All the quantities l_j and h_j are then positive and the result can be re-

https://doi.org/10.1017/9781009401296.020 Published online by Cambridge University Press

summed if we take the Laplace transform with respect to l, i.e.

$$\begin{aligned} \mathcal{N}(L,h) &= \int dl \exp(-lL) N(l,h) = \exp[hI(L)], \\ I(L) &= \int \bar{\alpha} dl \exp(-lL) \exp(-\bar{\alpha} l^2) \end{aligned} \tag{20.13}$$

This means that for a fixed value of $h = \log p_\perp^2$ we may by expansion in L obtain both the average value, $\langle l \rangle$, and the width, $\sigma(l) = \sqrt{\langle l^2 \rangle - \langle l \rangle^2}$ reached by $l = \log(1/x)$ after an arbitrary number of steps, starting from $x \sim 1$. These results are similar to the ones obtained for the λ-measure in Chapter 18:

$$\langle l \rangle = \frac{h}{2}, \quad \frac{\sigma(l)}{\langle l \rangle} = \sqrt{\frac{1}{h}\left(\frac{\pi}{\bar{\alpha}}\right)} \tag{20.14}$$

This means that the average rapidity (remember that $l = \log(1/x) = \log P_+ - y - \log q_\perp$) will in this way behave as

$$\langle y \rangle + \log q_\perp^2 = C \tag{20.15}$$

where C is a constant, $\log(\mu P_+)$, and μ is some length scale which cannot be determined by the present method. *This is just the cutoff line occurring in the SRM*, as we have shown above. We also note that the relative width decreases with h (although at present energies the width is still rather large).

From an investigation of Fig. 19.7 we conclude that the average line described by Eq. (20.15) is always at the top of the region forbidden by the non-local form factor of Marchesini *et al.* We have used a constant value of α_s but we note that a running coupling will bring us down from the SRM cutoff line.

Evidently this result depends upon the fact that we have taken all the $p_{\perp j}$ as increasing with j, i.e. all the h_j as positive. If some of the numbers h_j are positive and some are negative (which means that the main-line transverse recoil is no longer dominated by the last emission) then there are further contributions to the integrals. It is, however, easily seen that for a fixed value of h such contributions will produce a larger value of l, i.e. we will then be even more below the SRM suggestion.

The intention of this subsection is not to prove that the SRM results are identical to the CCMF results but instead to show that there must be necessary damping properties in connection with the gluon emissions in the DIS states. In the next section we will show that the CCMF model can be reformulated into a set of linked dipoles instead of a single 'extended' dipole with SRM damping.

https://doi.org/10.1017/9781009401296.020 Published online by Cambridge University Press

20.7 The linked dipole chain model

1 Introductory remarks

In the last section we have seen that the CCMF model, described in detail in section 19.6, implies results similar to those of the soft radiation model (SRM). The CCMF model contains a consistent description of the coherence conditions for QCD bremsstrahlung and includes the virtual corrections to the choice of ISB radiation in the model, cf. Eq. (19.2), in terms of the non-eikonal form factor. The SRM, however, stems from considerations of the behaviour of the radiation from an extended dipole. In this section we will show that the emerging 'extended dipole' picture of the radiation in the DIS states can be made even more precise, [16], i.e. *it is the radiation from a set of linked (color-connected) dipoles produced in a stochastical ISB scenario.* In order to obtain this result, the linked dipole chain (LDC) model, it turns out that the choice of ISB gluons must be restricted compared to the CCMF model.

To define the LDC model we recall that in the CCMF model, [44], the way to define the ISB is (i) to order all radiation in rapidity and (ii) to choose the ISB emissions as those that are not followed by a larger p_+-emission in this rapidity ordering (this is from the 'target' side, see Figs. 19.1 and 19.7). All the remaining radiation is included in the final-state bremsstrahlung (FSB). We also recall the particular requirement in Eq. (19.48) involving the fractional variable z_j and the transverse momenta of the jth emitted gluon, $p_{\perp j}$, and the ensuing propagator $q_{\perp j}$:

$$q_{\perp j}^2 > z_j p_{\perp j}^2 \tag{20.16}$$

The rapidity ordering is introduced to fulfil the strong angular ordering, i.e. the QCD coherence conditions for the bremsstrahlung emission. Increasing rapidity from the target side corresponds to decreasing angles along the emission line. It is, however, equally possible to order the emissions in rapidity from the probe side (we have already used this in connection with the description of the Webber-Marchesini model in section 17.7). Then the opposite rapidity ordering must be used and for every exclusive (i.e. fully defined) partonic final state the ISB should be chosen from a p_--ordering in the CCMF model formalism. A particular exclusive state will then contain a different set of ISB gluons and this results in a different non-eikonal form factor and a (seemingly) different contribution from the state to the cross section, cf. the discussion after Eq. (19.2).

We have already considered this question in detail in section 19.2 and we note that if the ISB gluons are more restricted then the $Sud(I)$ factors in Eq. (19.2) will generally be larger. It is a challenge to be able to partition the total state weight into a simple weight factor for the ISB, in

https://doi.org/10.1017/9781009401296.020 Published online by Cambridge University Press

accordance with QCD coherence, and at the same time obtain a simple description of the corresponding FSB gluons, given this ISB choice. One such approach is the LDC model, which exhibits the following features.

LDCa The final-state bremsstrahlung (FSB) correspond to emission from a set of color dipoles, spanned by the chosen gluons in the ISB set. Therefore the FSB can be treated by means of the Lund dipole cascade model (the DCM) (implemented in the Monte Carlo simulation program ARIADNE and described in detail in Chapter 17).

LDCb The inclusive weights for the ISB set of states chosen in the LDC model are simpler than the results for the CCMF model. The stochastical process obtained is, further, explicitly *local* (Markovian) and (in the leading-log approximation) symmetric with respect to emissions from the hadron and the probe end. In this way the predictions of the linked dipole chain model can be easily implemented in Monte Carlo simulation programs to study the particular ISB sets of the model.

LDCc It is possible to incorporate into the formalism both the ordinary perturbative QCD parton interactions, the boson-gluon fusion interactions and also the resolved (virtual) probe structure functions, including Rutherford interactions between the probe and the hadron ends. One consequence is that in the linked dipole chain (LDC) model there is no need of a cutoff (besides energy-momentum conservation) for large transverse momenta in the ISB gluon emissions, because such situations pass over in a well-defined way into Rutherford scattering. Correspondingly the gluonic bremsstrahlung also in a well-defined way defines a cutoff for small-transverse-momentum Rutherford scattering.

These statements will be clarified below. The model is defined in subsection 2 and in subsections 3 and 4 there is a description of the states in the triangular phase space as well as a discussion of how to generalise the model outside the leading-log approximation. Then the different channels are described in subsection 5 and finally, in Section 20.8, some features of the resulting structure functions are derived, in particular the relationship to the BFKL and DGLAP mechanisms, which we described in Chapter 19.

2 *The definition of the LDC model*

In [16] the LDC model is defined by the following restriction of the ISB gluons, compared to the CCMF model:

$$\begin{aligned} p_{\perp j}^2 &\geq \min(q_{\perp j}^2, q_{\perp j-1}^2) \\ &\simeq \min(-q_j^2, -q_{j-1}^2) \end{aligned} \tag{20.17}$$

https://doi.org/10.1017/9781009401296.020 Published online by Cambridge University Press

(The first line is defined by the Lorentz frame under consideration; the second is a Lorentz-invariant definition, which is approximately the same in the coordinate frames we have called 'equivalent to the hadron-probe cms' in Section 19.4.) Then it is possible to re-sum the weight in the emission step j of the CCMF model, Eq. 19.49, into

$$\bar{\alpha}\left(\frac{dz_j}{z_j}\right)\frac{dp_{\perp j}^2}{p_{\perp j}^2} = \begin{cases} \bar{\alpha}g_j d[\ln(1/z_j)]d\kappa_j & \text{if } \kappa_j > \kappa_{j-1} \\ \bar{\alpha}g_j d[\ln(1/z_j)]d\kappa_j \exp(\kappa_j - \kappa_{j-1}) & \text{otherwise} \end{cases} \tag{20.18}$$

Here on the right-hand side the constraint in Eq. (20.17) is introduced and we use $\kappa = \log q_\perp^2$. The quantity g_j corresponds to the azimuthal-angle (ϕ) average of the pole term $p_{\perp j}^2 = (\mathbf{q}_{\perp j} - \mathbf{q}_{\perp j-1})^2 = q_{\perp j}^2 + q_{\perp j-1}^2 - 2q_{\perp j}q_{\perp j-1}\cos\phi$, with the constraint in Eq. (20.17), using $a_j = \min(q_{\perp j}, q_{\perp j-1})/\max(q_{\perp j}, q_{\perp j-1})$:

$$g_j(a_j) = \frac{1}{2\pi}\int \frac{d\phi}{1 + a_j^2 - 2a_j\cos\phi}\Theta(a_j - 2\cos\phi) \tag{20.19}$$

It is straightforward to calculate the integral and we obtain

$$(1 - a_j^2)g_j(a_j) = \begin{cases} 1 - \frac{2}{\pi}\arctan\left[\frac{(1+a_j)\sqrt{2a_j-1}}{(1-a_j)\sqrt{2a_j+1}}\right] & 1 > a_j > 0.5 \\ 1 & 0.5 > a_j > 0 \end{cases} \tag{20.20}$$

To prove these statements it is necessary to carefully disentangle the contributions from the gluon emission in the CCMF model and sum over the non-eikonal form factor, cf. Eqs. (19.49), (19.50), for those which do not fulfil Eq. (20.17). Further it is necessary to convince oneself that it is possible to emit all the remaining gluons as FSB radiation from the dipoles between the chosen ISB gluons. We will consider these results in subsections 3 and 4, but in the remainder of this subsection we will investigate the consequences of the local stochastical process, which is symmetric with respect to the target and probe side defined by Eqs. (20.18) and (20.20).

'Local' means that the dipoles are determined by a Markovian stochastical process in the variables z, κ. With the $q_{\perp n}$-values and $x_n(= \prod^n z_j)$-values already obtained the next value of $q_\perp$ and a value of z can be chosen according to Eq. (20.18), e.g. by Monte Carlo simulation routines. The gluon $p_\perp$ is then defined by Eq. (20.17), its value of $(1-z)\prod^n z_j$ computed and we may then easily generate a dipole chain as shown in Fig. 20.8.

There is complete symmetry with respect to the target and the probe side, i.e. the values of the splitting variable z may be chosen along the positive or negative lightcones as $z_\pm$ (for the definition, see below and subsection 3 and for a discussion of this choice, subsection 4); the variables $z_\pm$ define the 'steps', $\log(1/z_\pm)$. The value of $\log q_\perp^2$ then defines the 'height' of the propagator virtuality and finally the emitted gluons

https://doi.org/10.1017/9781009401296.020 Published online by Cambridge University Press

(extended folds) are placed in an almost obvious way (for details, see the discussion in subsection 3).

There is a subtle but necessary change when we consider the production process from the probe side towards the target. The energy-momentum conservation equations at every vertex are written as $q_{j-1} = q_j + p_j$ and the index is increased from the target side. From the probe side we should, according to our convention, decrease the (propagator) indices, i.e. we must rewrite the relations as $-q_j = -q_{j-1} + p_j$ and generate 'negative' propagator vectors, but this is of course no problem (as they are all spacelike).

In Section 20.6 we noted the stepwise character of the process, i.e. that the splitting variable $z \ll 1$, in general. Then the positive and negative lightcone components fulfil $q_{+(j-1)} \gg z_{+j} q_{+(j-1)} = q_{+j} \simeq p_{+(j+1)}$ and $-q_{-(j+1)} \gg -z_{-j} q_{-(j+1)} = -q_{-j} \simeq p_{-j}$. Therefore the off-shell propagator vectors q_j are shown in Fig. 20.8 as horizontal lines between the two color-adjacent gluon emissions which form the dipole, with $-q_j^2 = -q_{+j} q_{-j} + q_{\perp j}^2 \simeq q_{\perp j}^2$.

In the next subsection we will consider the geometry of the triangular phase space for the emerging dipole chain. Although we have considered gluon emission within this phase space before, the situation for the bremsstrahlung in deep inelastic scattering is kinematically more complex.

3 *The geometry of the triangular phase space for DIS events*

In this subsection we will consider in some detail part of Fig. 20.8, in order to get acquainted with the way in which an emerging state in DIS is described in the triangular phase space of the LDC model. We concentrate on a dipole spanned between the emitted gluons p_1, p_2, with propagators q_1, q_0, q_2 in accordance with Fig. 20.9(*a*).

We note that the propagator q_0 is in between the massless gluons and we have chosen to exhibit the state in such a way that the propagator sizes are ordered as $-q_1^2 < -q_0^2 < -q_2^2$. (Exchanging the indices 1 and 2 would correspond to exchanging the probe and hadron side in the following arguments.) As the propagator sizes are dominated by the transverse momenta in most Lorentz frames (see below) we obtain, according to Eq. (20.17), $p_{\perp 1} = q_{\perp 0}$ and $p_{\perp 2} = q_{\perp 2}$. This is the most general situation possible (with obvious changes if we exchange the probe and the target sides) apart from the case when $p_{\perp 1} \simeq p_{\perp 2} \simeq q_{\perp 0} > \sqrt{-q_2^2}$, which, as we will later see, corresponds to a Rutherford scattering contribution (for the remainder of the discussion it is useful to note that in the LLA the inequalities $<$ can be exchanged for $\ll$, and $\simeq$ for equality).

The first observation is that there is a simple relationship between the variables $z_\pm$ corresponding to the splitting variables in the two different

https://doi.org/10.1017/9781009401296.020 Published online by Cambridge University Press

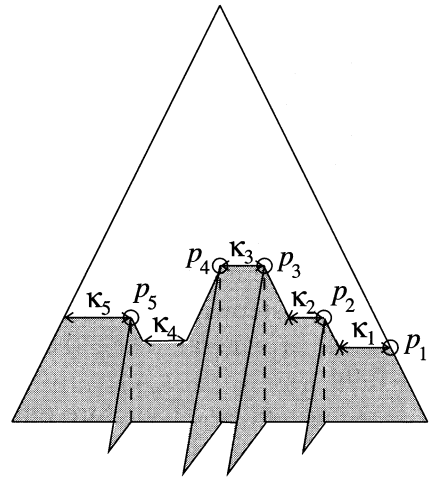

Fig. 20.8. A fan diagram in the LDC model as described in the triangular phase space. The extended folds correspond to on-the-mass-shell gluons and the arrows to the connector propagators. The front (back) borderline of the total triangle corresponds to the phase space boundaries, i.e. $\log P_+$ ($\log Q_-$) for the parton (probe).

directions, since for z_+, $q_1 \to q_0 p_1$ and for z_-, $-q_2 \to -q_0 p_1$. From the figure we may read off

$$\log(1/z_-) - \log(1/z_+) = \log(-q_2^2/-q_0^2) \tag{20.21}$$

(it is useful to relate this result to the requirement in Eq. (20.16)!).

According to perturbative QCD we may consider the state as resulting from the scattering of the two propagators $q_1, -q_2$, considered as the incoming entities, with the exchange of q_0 to obtain in the final state the two emitted gluons p_1, p_2, according to Fig. 20.9(b). (The minus sign in $-q_2$ is introduced to keep to energy-momentum conservation, as mentioned at the end of the last subsection, i.e. $q_1 - q_2 = p_1 + p_2$.)

While the triangular dipole phase space is manifestly invariant under Lorentz boosts along the chosen axis (i.e. the rapidity $y \to y + y_b$ with y_b, the boost rapidity, such that all rapidity differences stay constant) it is not so with respect to transverse boosts. We will therefore consider the scattering in two different, transversely boosted, Lorentz frames and also construct an approximate transformation between the frames in order to be able to understand the distribution in the triangular phase space.

As the dominating virtuality is $-q_2^2$ we will make the approximation $-q_1^2 \simeq q_{\perp 1}^2 \simeq 0$, using the LLA. We have then a dynamical situation

https://doi.org/10.1017/9781009401296.020 Published online by Cambridge University Press

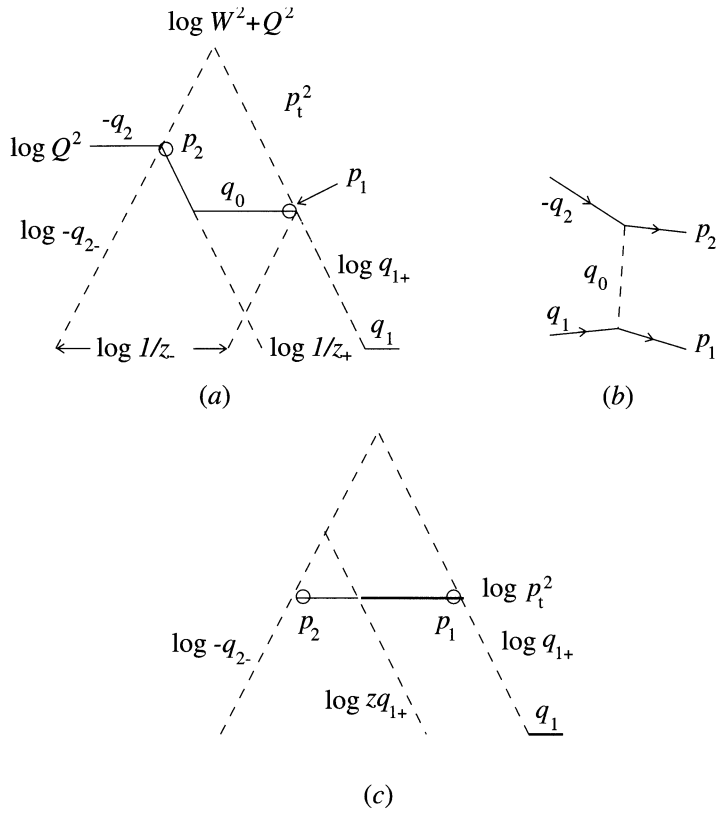

Fig. 20.9. A description of part of the fan diagram in the triangular phase space: (*a*) the three propagators q_1, q_0, q_2, denoted by lines, and the two emitted gluons p_1, p_2 of the dipole, for simplicity denoted by circles (although they correspond to triangular folds); (*b*) the corresponding scattering situation; (*c*) the resulting configuration in the probe($-q_2$)-parton(q_1) cms frame.

similar to deep inelastic scattering with $-q_2$ as the probe and the other three entities as massless particles. In the first frame the probe virtuality $-q_2^2 \equiv Q^2$ will correspond to a strong transverse momentum pulse $Q^2 \simeq q_{\perp 2}^2 = p_{\perp 2}^2 \gg p_{\perp 1}^2 = q_{\perp 0}^2$. *Then the situation is similar to the description of a DIS event in the lepton-parton cms frame.* In this frame the lepton and hadron approach each other along an axis. After the encounter the lepton recoils with a large transverse momentum $-\mathbf{p}_{\perp 2}$. The field probe (emitted by the lepton), $-q_2$, then transfers the final-state parton, indexed 2, to $\simeq \mathbf{p}_{\perp 2}$. (The notation $\simeq$ is used because there is also some transverse momentum flowing through the propagator q_0 to p_1.)

https://doi.org/10.1017/9781009401296.020 Published online by Cambridge University Press

With a dipole mass $(p_1+p_2)^2 = W^2$ we obtain, for the Bjorken variable, $x = Q^2/(Q^2+W^2)$. In order to interpret this variable in the triangular phase space we neglect in this frame the variables $q_{+2} \simeq q_{-1} \simeq 0$ (i.e. we assume that in the production of the dipoles before and after the one under consideration the splitting variables $z \ll 1$). Under those circumstances we obtain from energy-momentum conservation $q_{+1} \simeq p_{+1} + p_{+2}$ and $-q_{-2} \simeq p_{-1} + p_{-2}$ so that we may make the approximation

$$W^2 + Q^2 \simeq (p_1+p_2)^2 + (\mathbf{p}_{\perp 2})^2 \simeq -q_{+1}q_{-2} \tag{20.22}$$

From Fig. 20.9(a) we find, using Eq. (20.22), that the variable $\log(1/x)$ approximately equals the splitting variable $\log(1/z_+)$.

We will next consider the scattering in a frame where the two propagators have vanishing transverse components and lightcone components

$$q_{+1} = \frac{W^2+Q^2}{W}, \quad q_{-1} = 0, \quad q_{+2} = \frac{Q^2}{W}, \quad q_{-2} = -W \tag{20.23}$$

Remembering the minus sign we conclude that these are the probe($-q_2$)-parton(q_1) cms coordinates, i.e. we are using a description of the DIS event similar to the one in Section 19.4 (cf. Fig. 19.3). The final-state energy-momentum vectors will after the exchange of q_0 be (using $\mathbf{q}_{\perp 0} \equiv \mathbf{p}_\perp$)

$$\begin{aligned} p_{+1} &= q_{+1}(1-z), \quad p_{-1} = \frac{p_\perp^2}{p_{+1}}, \quad \mathbf{p}_\perp \\ p_{+2} &= \frac{p_\perp^2}{p_{-2}}, \quad p_{-2} = \frac{(W^2+Q^2)(1-z)}{W}, \quad -\mathbf{p}_\perp \end{aligned} \tag{20.24}$$

Energy-momentum conservation provides the following formula for the exchanged transverse momentum $p_\perp$:

$$p_\perp^2 = \frac{[zW^2 - (1-z)Q^2](W^2+Q^2)(1-z)}{W^2} \tag{20.25}$$

and we also note that the total virtuality of the q_0-propagator is

$$\begin{aligned} -q_0^2 &= \frac{p_\perp^2}{(1-z)} = \frac{zW^2 - (1-z)Q^2(W^2+Q^2)}{W^2} \\ &\equiv \frac{(W^2+Q^2)(z-x)}{(1-x)} \end{aligned} \tag{20.26}$$

where we have introduced the value of x defined before.

There are a few conclusions to be drawn immediately.

I From the expressions for $p_\perp^2$ and $-q_0^2$ we conclude that the splitting variable actually must be $z_+ = z > x$, and also that for fixed values of W and Q, z must grow with the value of the propagator $-q_0^2$. A closer analysis of the components of the momentum transfer q_0 tells

https://doi.org/10.1017/9781009401296.020 Published online by Cambridge University Press

us that $-q_{+0}q_{-0} = zp_\perp^2/(1-z)$ so that unless $z < 1-z$ this part of the propagator size $-q_0^2$ will dominate over the transverse momentum part $-p_\perp^2$. We will analyse the occurrence of large values of z in the next subsection. Remember that the possibility of large z-values implies problems for the BFKL mechanism in the x-development of the structure functions, cf. Section 19.5.

II When we compare the configuration in Fig. 20.9(a), where $-q_2$ brings p_2 to the same transverse momentum, $p_{\perp 2}^2 \simeq Q^2 > -q_0^2$, as that in the second frame, cf. Fig. 20.9(c), there are some differences. The emitted gluon vectors in the final state, p_1, p_2, are both placed, in the second frame, at the same $\log p_\perp^2$-level, corresponding to the exchanged transverse momentum in the propagator q_0. While p_1 has basically the same position as before, p_2 has moved down along the lightcone line $\log|q_{-2}|$, i.e. it has a smaller transverse momentum. (It is useful to consider the appearance of the dipole having q_2 as the propagator in the new frame!)

III While the second frame is a rest frame for the dipole the main axis is not along the dipole axis. The vectors $\mathbf{p}_1 = -\mathbf{p}_2$ form an angle with the main axis and also have an azimuthal angular difference π; note that in the triangular phase space each point in general corresponds to all azimuthal angles around the main axis! It is instructive to perform the necessary rotation to make the dipole axis the main axis. We will find that while the dipole axis in the first situation is a smooth curve from the positions of p_1 to p_2, although with a dip at the centre corresponding to approximately vanishing transverse momentum, in the new frame the two axes are exchanged.

Next we will construct an approximate Lorentz transformation between the dipole rest frame and the lepton-hadron cms in Fig. 20.9(a). To that end we start in the cms with the axis along the dipole axis so that $p_{+1} = p_{-2} = W$; we then boost along the positive axis to obtain $p_{+1}^{(1)} = \exp(-y_1)p_{+1}$, $p_{-2}^{(1)} = \exp(y_1)p_{-2}$, with a large boost rapidity y_1; see the treatment of such boosts in Chapter 2.

Then we perform a transverse boost to obtain a large $|\mathbf{p}_{\perp 2}^{(2)}| \equiv Q$ along some azimuthal direction. Finally we perform (in this new frame) a boost along the original dipole axis to obtain the vector $p_2^{(3)} \simeq (Q^2/W, W, \mathbf{Q}_\perp)$ while $p_1^{(3)} \simeq (W, 0, \mathbf{0}_\perp)$; in both cases we use lightcone coordinates and there are corrections of order $\exp(-2y_1)$.

It is now of interest to investigate what the transformations defined above will do to the points in the triangular phase space. Suppose that we take a (lightlike) vector approximately equal to p_2; the simplest example would be $p_2' = \zeta p_2, 0 < \zeta < 1$. The three Lorentz transformations we have

https://doi.org/10.1017/9781009401296.020 Published online by Cambridge University Press

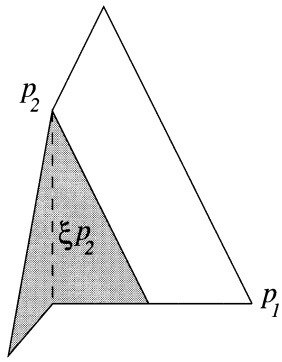

Fig. 20.10. The result of Lorentz transformation between the p_1p_2-dipole rest frame and a transversely moving frame, as described in the text.

described above will evidently transform it into $\zeta p_2^{(3)}$, i.e. with increasing ζ-values it will move from the baseline up along the triangle corresponding to p_2, see Fig. 20.10. Similarly the lightlike vectors (close to p_2) with small but nonvanishing transverse momenta (and azimuthal angles along and opposite to the boost direction) will fill in the region around this middle line (the shaded region in Fig. 20.10). Thus the shaded area, which comes to an apex at p_2, corresponds to the vectors which are collinear to p_2.

The reason for doing this transformation exercise for the points in the triangular phase space is to be able to describe the role of the virtuality $-q_0^2$ for the dipole spanned by p_1, p_2. In the dipole chain, shown in Fig. 20.8, we note that only final-state bremsstrahlung (FSB) is allowed within the shadowed region below the corresponding propagator. For the cases denoted by the indices $1, 2, 4$ the regions are bounded either by broken (logarithmic lightcone) lines, starting on the emitted gluons, or by the line corresponding to $\log(-q_j^2) \simeq \log(q_{\perp j}^2)$.

According to the results above it is the FSB emission, which is collinear to an original ISB gluon, that will cover the first kind of region, i.e. those FSB gluons that are produced close to the ISB gluon.

Actually it is straightforward to convince oneself that

FSB1 if we allow all possible bremsstrahlung in the rest frame of the dipole with $p_{\perp FSB} \leq \sqrt{-q^2}$ (q being the energy-momentum of the propagator in the relevant dipole) and

FSB2 if we then transform back to the original, i.e. the externally defined, frame

https://doi.org/10.1017/9781009401296.020 Published online by Cambridge University Press

then the FSB gluons will cover just the region below the broken lines and the logarithmic virtuality $\log(-q^2) \simeq \log q_\perp^2$.

4 The role of the virtuality and the possible extensions

According to the subsections above, in the LDC model the FSB is the radiation which can be emitted from the dipoles spanned by two adjacent initial state bremsstrahlung (ISB) partons. Each dipole can be characterised by two parameters, its mass, describing the size of the related triangular phase space, and its virtuality, i.e. the $-q^2$-size of the propagator which defines the largest transverse momentum allowed for FSB in the rest frame of the dipole. We will in this subsection provide a physical argument for the ocurrence of the virtuality cutoff and after that consider both the occurrence of large z-values and the possibility of extending the model outside the leading-log approximation (LLA).

In the description of timelike partonic cascades, which we encountered in e^+e^- annihilation events through the dipole cascade model (DCM), see section 17.2, there is a corresponding notion, i.e. no new emission is allowed with a transverse momentum above the earlier emission (the earlier emission may often define the dipole as such and the $p_\perp$-ordering corresponds to the coherence conditions of the radiation). The result that there can be no emission above the propagator $-q^2$ is, in connection with DIS events, a major result in the CCMF model, see section 19.6, and we will now outline a dynamical argument for this feature.

If we go back to the definition of a propagator in the Feynman way, cf. section 3.3, in particular subsection 3, we find that it describes the field activity inside a region compatible with Heisenberg's indeterminacy relations. If we use a coordinate system such that the energy-momentum-space propagator size $-q^2$ is essentially transverse, i.e. $-q^2 \simeq q_\perp^2$, then the size of the corresponding coordinate-space region is given by the canonically conjugate variable, i.e. the impact parameter b.

The occurrence of a particular $-q^2$-value consequently corresponds to a coordinate-space transverse distance $b \simeq 1/\sqrt{-q^2}$. Therefore the propagator size implies that *the two partons forming the dipole do not stem from a pointlike region*, i.e. there is a transverse distance between the emerging parton currents. In the soft radiation model in Section 20.5 we have already considered the radiation from an extended 'antenna'. *The result, that there is no emission with transverse momentum above the propagator* $-q^2 \geq p_{\perp FSB}^2$, *is due to the same extension property*, cf. Eq. (20.8). All radiation with a wavelength smaller than the typical size of the emitter is (form factor) suppressed. In the logarithmic phase space this implies at least exponential suppression, which in the LLA corresponds to a vanishing result. In the language of the CCMF model, [44], the

https://doi.org/10.1017/9781009401296.020 Published online by Cambridge University Press

same property is phrased as follows: above the propagator virtuality real emission is cancelled by the virtual corrections.

We note that the present results are only valid in the leading-log approximation (LLA). It is tempting to extend the model beyond the LLA by the use of the 'true' splitting functions $\mathscr{P}(z)$, see Eq. (19.30), instead of the $1/z$-pole. There are then a set of problems to be faced. In order to resolve them we will make use of the scattering results of subsection 3 above and the derivation of the splitting functions in Section 17.7.

The first problem we encounter is whether we should interpret the splitting variable z as z_+ or z_-, i.e. in the notation above whether we should consider the process from the target or from the probe side. To resolve that question we consider Fig. 19.6 and note that in the derivation of the splitting functions, see e.g. Eq. (17.25), the incoming parton is assumed to be massless. In Fig. 19.6 it is denoted by its lightcone energy-momentum fraction $x' \equiv q'_+/P_+$, with P_+ the (target) parton energy-momentum. It is split up into a parton, with $x \equiv q_+/P_+ = zx'$, assumed to have a (large) virtual mass, $-Q^2$, and another massless parton with $x_g = (1-z)x'$. Then the variable z equals $z_+ \equiv q_+/q'_+$, i.e. the positive lightcone energy-momentum ratio of the consecutive propagator vectors.

Thus if we increase the virtuality from the target side, which in the notation above means that $\kappa_{j-1} < \kappa_j$ (examples in Fig. 20.8 are $\kappa_1 < \kappa_2 < \kappa_3$ and $\kappa_4 < \kappa_5$) – note that this means going 'down' in virtuality from the probe side! – then we should use z_+. In the opposite case, i.e. when we go down from the target side, which means that we go up from the probe side (the example in Fig. 20.8 is $\kappa_4 < \kappa_3$) then we should evidently use $z = z_-$ in order to keep to this virtuality ordering.

But there is another and more difficult problem. Besides the z-pole the splitting functions, $\mathscr{P}(z)$, contain some finite corrections and even a $(1-z)$-pole, cf. section 17.7. We have already discussed the $(1-z)$-pole in connection with the DGLAP mechanism (where it is formally regularised by means of the Sudakov factor or physically by energy-momentum conservation). Within the BFKL mechanism there is a problem if the bremsstrahlung emissions stem from large z-values, cf. section 19.5. In order to investigate the occurrence of large z-values we return to the results of subsection 3.

From Eqs. (20.23)–(20.26) we may read off the behaviour of the emitted gluon vectors p_1, p_2 for all values of z, see Fig. 20.11. The size of $-q_0^2$ will increase with z (for fixed W, Q) and be equal to $-q_2^2 = Q^2$ for $z = z_1 = x(2-x)$ (which satisifes $1 \geq z_1 \geq x$ as it should). Further, the two vectors p_1, p_2 will be described by the same point in the triangular phase space when $z = z_2 = (1+x)/2$ (note that $1 \geq z_2 \geq z_1$). At this point the scattering situation corresponds in the cms to a scattering angle $\theta = \pi/2$, (it is straightforward to see that $p_{+j} = p_{-j} = p_{\perp j}$, $j =$

https://doi.org/10.1017/9781009401296.020 Published online by Cambridge University Press

1, 2), i.e. the vectors $\mathbf{p}_j$ are transversely directed, with opposite azimuthal angles.

If z increases further *the two vectors p_1, p_2 change place with respect to rapidity ordering in the triangular phase space.* We obtain a situation similar to that discussed in Section 15.4, in particular in subsection 1, and in Section 17.8, i.e. that the color-field flow is not stretched along the 'simplest' direction between the emitted partons in a cascade, see Figs. 15.8 and 20.11(b). *This is a forbidden configuration in a strictly strong-angular ordering scenario* but, although in general strongly suppressed, it is often an allowed configuration when QCD coherence is not taken approximately; we are after all working in a three-space-dimensional world!

When we continue, for values of $z > z_2$, the situation corresponds to backwards scattering with a cms scattering angle $\theta > \pi/2$. The transverse momenta of the two p_j-vectors decrease *but the propagator size $-q_0^2$ increases to $-q_{0max}^2 = Q^2 + W^2$.* The development for increasing z-values is shown in Fig. 20.11(a). Within our present knowledge, which comprises the results from the analysis in the CCMF model, there is no indication of the way to treat this situation. We only know that it must be suppressed owing to the difficulty of fulfilling the QCD coherence conditions.

We should also be aware, however, that color coherence may not be only a question of angular ordering when we consider the development along a line with gluon quantum numbers, i.e. when there is both a color and an anticolor line along the propagator chain and the emitted partons are gluons. It is straightforward to convince oneself that in half the cases the two (adjacent) gluons p_1, p_2, which we have considered repeatedly, will have a color charge in common but in the remaining cases they correspond to emissions from the two independent color lines of the propagator; the two situations are shown in Fig. 20.11(c) but at the present time we will have to leave the above-mentioned question as an open problem.

There is one situation which we have up to now completely neglected and that is the gluon splitting process $g \to q\bar{q}$. As always it is only at a small percentage level compared to gluon emission $g \to gg$ and therefore is of minor interest along the emission chains. But it is of direct interest at the end of any fan diagram because an electromagnetic (as well as a weak-interaction) probe can only interact with the q- and $\bar{q}$-partons. We note that in this case there is no pole for the splitting variable so that z and $1 - z$ are in general of the same size, cf. Eq. (17.26).

We finally note another consequence of the scattering behaviour described above when $z_1 < z < z_2$ (which for small values of $x \simeq Q^2/W^2$ is essentially the whole available z-region $0 < z < 1$). In this case the two ISB gluons p_1, p_2 are both placed at the same $\log p_\perp^2 \simeq \log(-q_0^2)$ level, i.e. at the two edges of the largest propagator q_0 above $-q_2$. In this

https://doi.org/10.1017/9781009401296.020 Published online by Cambridge University Press

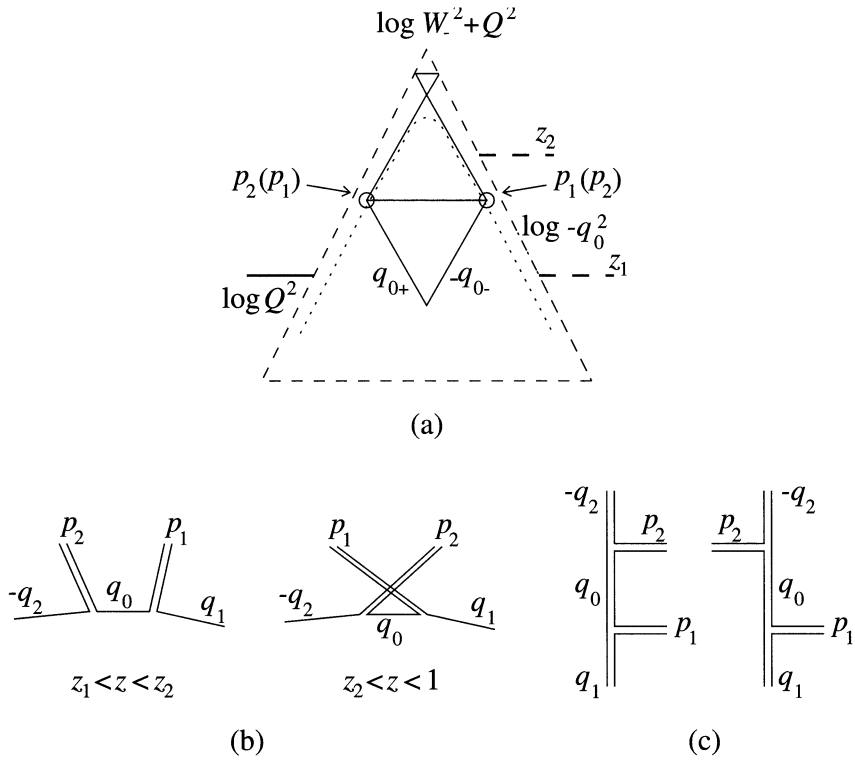

Fig. 20.11. (*a*) For small values of the splitting variable z the dipole virtuality size fulfils $-q_0^2 \simeq q_{\perp 0}^2 \gg -q_{+0}q_{-0}$ (the lower 'crossed' configuration) but for large z, $\log(-q_0^2)$ increases to the turning point $z = z_2$. For $1 > z > z_2$, $\log(-q_0^2)$ increases further but then $-q_{+0}q_{-0} > q_{\perp 0}^2$ (the upper 'crossed' configuration). The two cases correspond to the two color-line descriptions in (*b*). In (*c*) we have the two color-flow situations when there are gluons as 'in', 'out' and propagator partons.

situation the chain moves up and down in virtuality in a symmetric way from both the target and the probe side. *It corresponds to a Rutherford scattering interaction* like the one described in detail in Section 5.4. From the weight distribution in Eq. (20.18) we find that in the present case there will be a pole of the kind $(-q_0^2)^{-2} \simeq p_\perp^{-4}$ (there is one $p_\perp^{-2}$-factor from each side), in accordance with the results of Eq. (5.40)! Thus, as we will further discuss in the following subsections, *the ISB bremsstrahlung in the LDC model goes over to Rutherford scattering at the largest virtuality in the chain.*

https://doi.org/10.1017/9781009401296.020 Published online by Cambridge University Press

5 The different channels in deep inelastic scattering

In the analysis of the structure functions it is in general tacitly assumed that the major momentum transfer stems from the external probe, $-q^2 = Q^2$. As we have seen in the subsections above the LDC model contains the possibility of considering also situations where there is some virtuality along the chain which exceeds Q^2. Such situations are of interest in particular for small and moderate Q^2-values (with large cross sections at HERA) and we will in this subsection subdivide the DIS cross section into three channels with different properties in this respect:

I the usual quark-parton model interaction, in which the largest virtuality along the chain is given by Q^2,

II a boson-gluon fusion (BGF) event, in which the (final) propagator virtuality exceeds the probe virtuality $-q^2 \simeq q_{\perp n}^2 > Q^2$,

III a Rutherford parton-scattering event, in which there is one virtuality further down the chain, $q_{\perp max}^2$, exceeding all the remaining ones (note that there may in general be several 'local' maxima if the chains are sufficiently long, counted in $\log(1/x)$ units, but as such situations are very rare within the presently obtainable energy regimes we will neglect them).

In Fig. 20.12 the triangular phase space is again shown (we will subsequently use the probe-parton cms according to Section 19.4 and subsection 3 above) with the variables $\log(1/x_B)$ and $\log Q^2$ and with three 'chain-roads' as examples of the cases I–III. On the right-hand side of the figure we show the conventional Feynman diagrams for the three cases and the main momentum transfer is particularly emphasised.

The structure function f is for case I conventionally obtained from an integral over the last propagator $q_\perp \leq Q$ (here $x = \prod z_j = x_B$ and $\mathscr{F}$ is the so-called non-integrated structure function):

$$f(x, Q^2) = \int^{Q^2} \frac{dq_\perp^2}{q_\perp^2} \mathscr{F}(x, q_\perp^2) \tag{20.27}$$

Therefore in the probe-parton cms the chain will end somewhere along the (positive lightcone) line AB. Just like the emitted parton p_2 in the scattering discussion of subsection 3, the final-state parton, after absorption of the probe momentum, will keep the transverse momentum from the chain, i.e. $p_{\perp n+1} \simeq q_{\perp n}$, and end up at point E along the (negative lightcone) line CD, corresponding to the Q_- of the probe.

For the boson-gluon fusion event in case II we note that the last propagator will have $q_{\perp n}^2 > Q^2$ and also $q_{+n} = x_n P_+$ with $x_n = \prod z_j > x_B$. This last relation can be read off from Fig. 20.12 and can be understood

https://doi.org/10.1017/9781009401296.020 Published online by Cambridge University Press

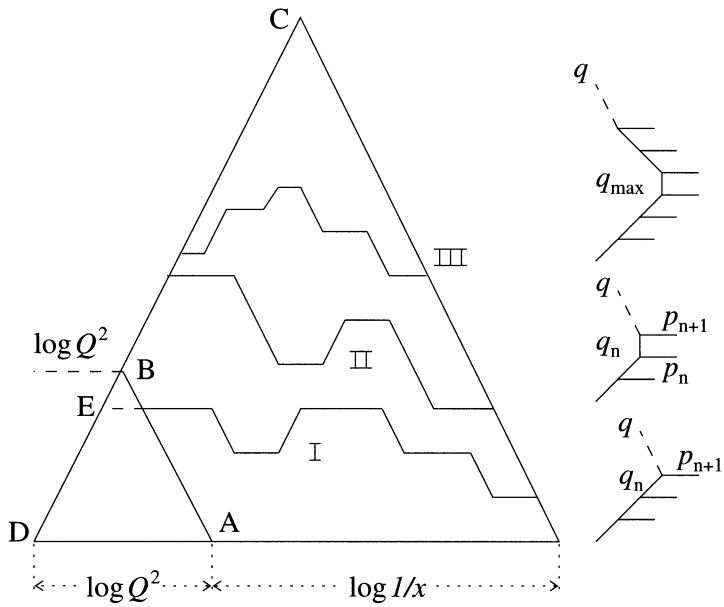

Fig. 20.12. Examples of the different kinds of fan diagram chain. Using $Q_+ = xP_+$ the baseline rapidity region is divided into $(-\log Q_-, \log Q_+)$ and $(\log Q_+, \log P_+)$ with lengths $\log Q^2$ and $\log(1/x)$, respectively.

from the following simple calculation. The last parton in the chain, see the second chain path in Fig. 20.12, will again have $p_{\perp(n+1)} \simeq q_{\perp n}$ and pick up the negative lightcone fraction of the probe, i.e. $p_{-(n+1)} \simeq Q_-$. Therefore energy-momentum conservation at the vertex $q_n \to -Qp_{(n+1)}$ provides, cf. the kinematics discussed in subsection 3 and in Section 19.4,

$$q_{+n} = -Q_+ + p_{+(n+1)} = \frac{Q^2}{Q_-} + \frac{p^2_{\perp(n+1)}}{p_{-(n+1)}} \simeq \frac{Q^2 + q^2_{\perp n}}{Q_-} \qquad (20.28)$$

We conclude that, while the first term in the last expression is by definition $x_B P_+$, in the boson-gluon-fusion situation the second term will dominate, i.e. $q^2_{\perp n} > Q^2$. We then obtain $q_{+n} \simeq p_{+(n+1)} = \prod(z_j)P_+ = x_n P_+ = xP_+ q^2_{\perp n}/Q^2$. We may go further and conclude that the definition of the non-integrated structure function can be extended from Eq. (20.27) to

$$f(x, Q^2) = \int \frac{dq^2_\perp}{q^2_\perp} \mathscr{F}(\hat{x}, q^2_\perp), \quad \hat{x} = \begin{cases} x_B & \text{if } Q^2 > q^2_\perp \\ x_B q^2_\perp / Q^2 & \text{otherwise} \end{cases} \qquad (20.29)$$

but we must then in the second equation remember that there is a factor $Q^2/q^2_\perp$ included in the last step for the non-integated $\mathscr{F}$, corresponding to

https://doi.org/10.1017/9781009401296.020 Published online by Cambridge University Press

the definition of the transverse momentum dependence in Eq. (20.17) (we must go downwards from $q_\perp^2$ to get to Q^2).

Finally for chain-road III with $q_{\perp max}$ exceeding all other momentum transfers the same argument provides for the non-integrated $\mathscr{F}$

$$\frac{Q^2}{q_{\perp n}^2} \times \frac{q_{\perp n}^2}{q_{\perp n-1}^2} \times \cdots \times \frac{q_{\perp j}^2}{q_{\perp max}^2} = \frac{Q^2}{q_{\perp max}^2} \tag{20.30}$$

i.e. a direct generalisation of the results for the boson-gluon-fusion events. As each step is weighted by $d\kappa = dq_\perp^2/q_\perp^2$ the Rutherford scattering result $dq_{\perp max}^2/q_{\perp max}^4$ will occur as soon as we reach a maximum and would like to go downwards along the chain. (An observant reader may note that the contributions appear in a non-symmetrical way with respect to the target and probe sides but an even more observant one will note that the structure function as it is defined is not a symmetric notion, cf. the discussion in section 20.8.)

The main result is, however, that the LDC chains include Rutherford parton-scattering contributions, too, and that the largest momentum transfer subdivides the event chain into one part stemming from the (coherent) bremsstrahlung from the parton while the other part can be attributed to the resolved probe. Thus *the largest transverse momentum of the bremsstrahlung chain(s) provides the lowest cutoff for Rutherford scattering, and conversely Rutherford scattering along a chain provides the upper cutoff for the bremsstrahlung.*

It is consequently possible to define a structure function for both the target and the projectile and then the notions of 'probe' and 'parton' are a matter of convention, because the cross section for the interaction corresponds to the convolution of these two structure functions together with the relevant Rutherford parton interaction.

20.8 The structure function behavior of the LDC model

1 Introduction

In this section we will provide a more detailed analysis of the properties of the structure functions than we have done before and in particular exhibit the combined role of the DGLAP and BFKL mechanisms for the final result (although we will find that over the HERA energy region the DGLAP mechanism will be the dominant one, except for such small Q^2-values that we cannot trust the results of perturbative QCD). To avoid confusion we repeat some of the notation. We use the ordinary DIS variables $W^2, Q^2, x_B = Q^2/(W^2 + Q^2)$. For the emitted massless gluon and the (spacelike) propagator vectors we use p, q, for the splitting variable and

https://doi.org/10.1017/9781009401296.020 Published online by Cambridge University Press

the transverse momenta we use $z, q_\perp, p_\perp$ and for the natural logarithmic variables we use $\ell \equiv \log(1/x_B), \kappa \equiv \log q_\perp^2, L_Q \equiv \log Q^2$.

2 *The integral equations for the non-integrated structure function*

The results of the earlier subsections can in a straightforward way be formulated as an integral equation for the non-integrated structure function $\mathcal{F}$, cf. Eq. (20.27), which actually is a function only of ℓ and κ:

$$\mathcal{F}(x, q_\perp^2) \equiv \mathcal{F}(\ell, \kappa) = \sum_{j=1}^{3} \mathcal{I}_j \tag{20.31}$$

The meanings of the the terms $\mathcal{I}_j$ are as follows.

$\mathcal{I}_1$ This is the possibility of taking a single step from a starting point (ℓ_0, L_{Q0}) (conventionally $\ell_0 = 0, L_{Q0} = 0$, which defines both the properties of the starting-point and the scale of the coupling), to the final point (ℓ, κ). It is a boundary term, $\mathcal{I}_1 = \bar{\alpha}$, in the integral equation.

$\mathcal{I}_2$ This is the possibility of being at a point (κ', ℓ') below κ, i.e. $L_{Q_0} < \kappa' \equiv \log q_\perp'^2 < \kappa$ and $\ell_0 < \ell' \equiv \log(1/x') < \ell = \log(1/x_B)$, and taking the final step to ℓ upwards in transverse momentum (as in the DGLAP mechanism). We obtain

$$\mathcal{I}_2 = \int_{L_{Q0}=0}^{\kappa} \bar{\alpha} d\kappa' \int_{\ell_0=0}^{\ell} d\ell' g \mathcal{F}(\ell', \kappa') \tag{20.32}$$

$\mathcal{I}_3$ This is the possibility of being at $\kappa' > \kappa$ and taking a step downwards to κ. Note the factor $q_\perp^2/q_\perp'^2 = \exp(\kappa - \kappa')$ in $\mathcal{F}$ and a compensating change $\ell' \to \ell' + \kappa - \kappa'$ according to Eqs. (20.18) and (20.29):

$$\mathcal{I}_3 = \int_{\kappa}^{\ell} \bar{\alpha} d\kappa' \exp(\kappa - \kappa') \int_0^{\ell+\kappa-\kappa'} d\ell' g \mathcal{F}(\ell', \kappa') \tag{20.33}$$

This is a leading-log approximation (LLA) equation. If we go further and neglect the variations around the pole and put $g = 1$, cf. Eq. (20.18) and the discussion below, it will be a symmetric (in mathematical terms 'Hermitian') integral equation in terms of the left-right (i.e. from the probe and parton side) symmetric non-integrated $\mathcal{F}_s \equiv \mathcal{F} \exp(-\kappa/2)$. (This is the lack of symmetry we noted in connection with the Rutherford contributions to the structure functions in subsection 4 of the last section.) We immediately recognize the DGLAP contribution in the first two terms, cf. Eqs. (19.33)–(19.35). We will next exhibit the corresponding BFKL contribution, in particular the Lipatov kernel, which was mentioned in section 19.5.

https://doi.org/10.1017/9781009401296.020 Published online by Cambridge University Press

Before we continue we note the starting point of the LDC model, i.e. that the transverse momentum generation stems from $d^2q'_\perp/[2\pi(\mathbf{q}'_\perp-\mathbf{q}_\perp)^2]$, the azimuthal angular average of the pole term $1/\mathbf{p}^2_\perp$ in the emission, as seen in Eqs. (20.18)–(20.20). The factor g contains the LDC requirement given in Eq. (20.17) but it is unity unless we are close to $\kappa \simeq \kappa'$, i.e. when the emitted gluon transverse momentum is very small, $p_\perp \simeq 0$.

In order to relate the pole term to the Lipatov kernel we use the following approximate relationship:

$$\frac{\mathscr{F}(\ell,\kappa')}{p^2_\perp}\Theta(p_\perp - q'_\perp) \simeq \frac{\mathscr{F}(\ell,\kappa') - \mathscr{F}(\ell,\kappa)\Theta(q_\perp - p_\perp)}{p^2_\perp} \tag{20.34}$$

If this is inserted into the integral equation Eq. (20.31) and the equation differentiated with respect to $\ell = \log(1/x)$ we obtain

$$\frac{\partial\mathscr{F}(\ell,\kappa)}{\partial\ell} = \int \frac{\bar{\alpha}d^2q'_\perp}{2\pi p^2_\perp}[\mathscr{F}(\hat{\ell},\kappa') - \mathscr{F}(\ell,\kappa)\Theta(q_\perp - p_\perp)] \tag{20.35}$$

which is almost the BFKL equation. The difference is the occurrence of $\hat{\ell} = \max(\ell, \ell + \kappa' - \kappa)$, i.e. the compensation in the contribution $\mathscr{I}_3$, which corresponds to the use of the relevant splitting variable z_- instead of z_+, cf. Eq. (20.21) and the discussion in subsection 4 of the previous section.

3 *The solutions to the integral equations*

Using the conventional methods for analysis, we will now investigate the solutions of Eqs. (20.31) and (20.35). To that end we introduce the moments of the non-integrated $\mathscr{F}_N$:

$$\mathscr{F}_N = \int dx\, x^{N-1}\mathscr{F} \tag{20.36}$$

and the *anomalous dimensions*, γ_N of this moment function:

$$\mathscr{F}_N \propto (q_\perp)^{2\gamma_N} = \exp(\gamma_N\kappa) \tag{20.37}$$

Insertion into Eq. (20.35) provides the following result:

$$1 = \frac{\bar{\alpha}}{N-1}\xi(\gamma_N) \equiv \frac{\bar{\alpha}}{N-1}[h(\gamma_N) - h(N-\gamma_N)] \tag{20.38}$$

The two h-terms in ξ stem from the the transverse momentum integrals in $\mathscr{I}_2$ and $\mathscr{I}_3$ from Eqs. (20.32) and (20.33). If we put $\hat{\ell} = \ell$ in Eq. (20.35), i.e. in practice neglect the difference between $z+$ and z_-, then the argument $N-\gamma_N$ in the second h-term of ξ becomes $1-\gamma_N$. This is a consistent procedure in the BFKL approach (to be called *conventional BFKL*) because the intention is to take into account the sub-leading contributions in the transverse momentum fluctuations while keeping to the $1/z$ pole in the longitudinal generation.

https://doi.org/10.1017/9781009401296.020 Published online by Cambridge University Press

It is straightforward to obtain the following expression for the function h (if we use Eq. (20.35), i.e. basically put $g = 1$ in Eqs. (20.18) and (20.31)):

$$h(\gamma) = \int_0^1 \frac{du(u^{\gamma-1} - 1)}{(u-1)} = \psi(1) - \psi(\gamma) \tag{20.39}$$

where ψ is the Euler function (the derivative of the logarithm of the Γ-function). There is a mathematical theorem by which we may invert the moment equation (20.36) to obtain a formula for $\mathcal{F}$ itself, including both the x_B- and the $q_\perp$-dependence. We will not write out the formulas but, as we have noted before, the major x_B-dependence will stem from the largest value of $N-1$ which is a solution to Eq. (20.38). For conventional BFKL any useful mathematical table will show that this occurs for $\gamma_N = 1/2$ and that for this value of $N = N_L$ (the Lipatov case)

$$N_L - 1 = 2\bar{\alpha}h(1/2) = 4\bar{\alpha}\log 2 \equiv \lambda_L \tag{20.40}$$

It is an interesting fact that this value of N_L corresponds to the place where the two solutions of Eq. (20.38) coincide, in accordance with the symmetry $\gamma \leftrightarrow 1-\gamma$. In the inverse moment integral we then have a singularity (the two poles, corresponding to the solutions, will approach their common value from each side of the integration contour and provide a 'pinch singularity'). While $\lambda_L \simeq 0.5$ in Eq. (20.40) (for $\bar{\alpha} = N_c\alpha_s/\pi \simeq 3/\pi \times 0.2$) the corresponding general solution of Eq. (20.38) (when the difference between z_+ and z_- is not neglected) corresponds to a pinch singularity for $\gamma = N/2$. Then the largest λ-value is diminished to $\lambda \simeq 0.31$!

We have already seen in section 19.5 that there are very large corrections to the BFKL mechanism (stemming from the contributions to the integrals for large values of of the splitting variables z). The result just mentioned corresponds to a different mechanism. If we allow for the simplest corrections, those subleading in N, to the BFKL eigenvalue equation (which recognise the fact that $z_+ \neq z_-$ in general) then we again obtain very large changes in λ. And these corrections will again result in essentially smaller effective λ-values!

4 *Further remarks on the solutions*

It is possible to continue the analytical investigations of the structure functions and e.g. to introduce the LDC requirement, which effectively means reintroducing the factor g in Eq. (20.18). But it is then necessary to take recourse to numerical calculations because the integrals no longer correspond to elementary functions. The result of such investigations are that for a sufficiently large value of $\log(1/x_B)$ there is always an approximate power behaviour, i.e. the gluon structure function $x_B g$ behaves as $x_B^{-\lambda_e}$ with an effective power $\lambda_e \simeq 0.3 \ll \lambda_L$. But for values of $\log(1/x_B)$ of the

https://doi.org/10.1017/9781009401296.020 Published online by Cambridge University Press

same order as $\log Q^2$ (cf. Fig. 20.12)) the DGLAP mechanism, leading to a structure function $x_B g \propto \exp[2\sqrt{\chi(Q^2)\log(1/x_B)}]$, cf. Eqs. (19.35)–(19.36), will be dominant (with a very slowly varying function $\chi(Q^2)$ and also a slow dependence on the proportionality constants).

We will end this investigation with a few simple analytical calculations to exhibit these facts. In the first we will find that for small $\kappa = \log q_\perp^2$ values the very construction of the LDC chains leads to a simple result of the BFKL kind. In the second we will nevertheless find that the BFKL mechanism is only relevant for very large values of $\ell = \log(1/x)$. Finally we will consider the effect of a running coupling on the LDC equations and show that *the BFKL diffusion effect in transverse momentum*, i.e. the gaussian $\log Q^2$ behaviour with a width proportional to ℓ mentioned in Section 19.5, is not consistent.

In the LDC model it is according to the earlier subsections possible to go up and down in κ along the chains. Let us consider all the possibilities of a *combined step-motion*, cf. Fig. 20.13: we consider the situations when there is one set of up-steps followed by another set of down-steps. Thus we start at $\ell_{+0} \equiv \ell_0 = L_{Q0} = 0$ and only follow (in κ) upwards directed chains to reach a stochastically chosen maximum point κ_1 at $\ell_{+1} \equiv \ell_1$. Then we continue (still from the target side) downwards to reach the final point $\ell_+ \equiv \ell$ at $\kappa < \kappa_1$ (note that the second part corresponds to up-steps from the probe side!).

We would like to obtain the total weight in the LDC model from all possible chains with this property. Then we have (from the target side) a DGLAP motion $(0,0) \to (\ell_1, \kappa_1)$ and from the probe side a corresponding DGLAP motion $(\ell_{-0} = 0, \kappa) \to (\ell_{-2} \equiv \ell_2, \kappa_1)$ (where $\ell_{-0}, \kappa_1)$ corresponds to the endpoint $\ell_+ \equiv \ell, \kappa$ and $\ell_{-2} \equiv \ell_2, \kappa_1)$ the maximum point $\ell_{+1} \equiv \ell_1, \kappa)$). From Fig. 20.13 we obtain

$$\kappa_1 = \kappa_2 + \kappa, \quad \ell_1 + \ell_2 + \kappa_1 = \ell + \kappa \tag{20.41}$$

We will use a fixed coupling $\bar{\alpha}$, which means that the DGLAP contributions for the two cases are $\exp(2\sqrt{\bar{\alpha}\ell_j\kappa_j})$, $j = 1,2$ (note that, for fixed coupling, $\chi = \bar{\alpha}\kappa$ according to Eq. (19.35)). For the symmetric non-integrated $\mathcal{F}_s$, defined above, we have the factors $\exp(-\kappa_j/2)$ from the transverse momentum generation and we are then supposed to sum over all contributions with the constraints in Eq. (20.41). Thus we have an integral in two independent variables, which may be chosen as e.g. ℓ_2 and κ_2:

$$\mathcal{F}_s = \int d\ell_2 d\kappa_2 \exp\left[2\sqrt{\bar{\alpha}\ell_2\kappa_2} + 2\sqrt{\bar{\alpha}(\kappa+\kappa_2)(\ell-\ell_2-\kappa_2)} - \kappa_2 - \kappa/2\right] \tag{20.42}$$

where we have introduced the constraints from Eq. (20.41). This integral

https://doi.org/10.1017/9781009401296.020 Published online by Cambridge University Press

can be solved by stationary-phase or equivalently saddle-point methods, i.e. we look for the maximum in the integrand exponent as we did when investigating the fragmentation function in the Lund model in Eq. (9.6). This time we have to consider the maximum with respect to two variables but after a little algebra we find the surprisingly simple result that

$$\mathscr{F}_s \simeq \exp[(R-1)(2\ell+\kappa)/4], \quad R=\sqrt{1+8\bar{\alpha}} \tag{20.43}$$

Thus *the symmetrical structure function only depends upon the rapidity difference* between the starting point and the endpoint, i.e. $\delta y \equiv \ell + \kappa/2$, cf. Fig. 20.13(*a*). This means that the result can be easily generalised to any number of added going-up and going-down cells. A closer examination tells us, however, that the maximum is only obtained within the integration region if ℓ is large compared to κ, i.e. if there is a sufficiently strong suppression of large κ-values. There will be a dividing line with

$$\kappa = \frac{R-1}{R}\delta y \tag{20.44}$$

(where R is defined in Eq. (20.43)) with the property that for smaller κ-values there is a maximum but for larger κ the main contribution is a single DGLAP motion always directed upwards in κ. It is interesting that we again meet a result very similar to the one obtained in the soft radiation model in section 20.5, i.e. a cutoff which can be formulated as in Eq. (20.10). (It is worthwhile to calculate the corresponding 'dimension' in the cutoff as a function of both $\lambda_e = (R-1)/2$ and $\bar{\alpha}$ and consider the consequences of the results!) Anyway for κ below the line the result is obviously of the BFKL kind, i.e. there is (besides the symmetrical κ-dependence) an effective $x^{-\lambda_e}$ behaviour, but this time with $\lambda_e = (R-1)/2 \simeq 0.3$ for our 'conventional' value of $\bar{\alpha} \simeq 3/\pi \times 0.2$.

The next calculation will provide a useful formula for the major contributions to the structure functions when we start at the point $\ell_0 = L_{Q0} = 0$ and make use of all possible paths that end on the point (ℓ, L_Q). It is actually only possible to perform the full calculation by means of numerical methods but the final result is sufficiently simple that the following considerations apply. Firstly it turns out that the major contribution also corresponds closely to the 'average' path. This average is obtained if, for a fixed value of the rapidity in the triangular phase space, we consider the average 'passage' κ-value; the averaging is done by means of the LDC weights in Eq. (20.18).

In Fig. 20.13 we show the results for the two cases when $L_Q \simeq \ell$ and when ℓ dominates L_Q (we also show the fluctuation bands around the average paths). The most noticeable property is that *if we use a running coupling* (which is the case in the figures) *then there is a preference for small $q_\perp$-values*. The major contribution stems from an average path that

https://doi.org/10.1017/9781009401296.020 Published online by Cambridge University Press

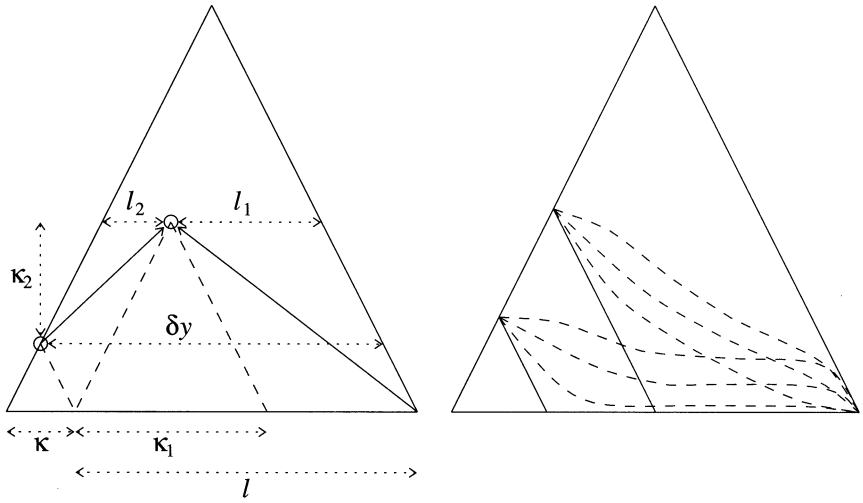

Fig. 20.13. (*a*) The combined DGLAP motion of one step (ℓ_1, κ_1) from the target and one step (ℓ_2, κ_2) from the probe, together forming $(\delta y, \kappa)$; (*b*) the average paths (together with the deviations) for a small and a large value of $L_Q = \log Q^2$.

stays close to $\kappa \simeq 0$ but, in the end, in order to reach the required L_Q goes up in κ. A simple assumption (which turns out to provide a very good approximation to the numerical results) is to subdivide the total $\ell = \log(1/x_B)$ into a 'first' BFKL contribution in ℓ_1, $\propto \exp(\lambda_e \ell_1)$ (close to the $\kappa = 0$ axis), times a DGLAP contribution in the 'final' ℓ_2-step upwards to L_Q, $\propto \exp[2\sqrt{\chi(Q^2)\ell_2}]$, and perform a convolution integral with the constraint $\ell_1 + \ell_2 = \ell$. It is easy (again using a stationary-phase method) to obtain that

$$\mathcal{F} \simeq \exp[\lambda_e \ell + \chi(Q^2)/\lambda_e] \tag{20.45}$$

if the saddle point $\ell_1 = \chi/\lambda_e^2$ is inside the integration region $0 < \ell_1 < \ell$. It is interesting to note that for a constant coupling $\bar{\alpha}$ we obtain back the division line in Eq. (20.44) if we use the value of λ_e defined by Eq. (20.43). For a truly running coupling, however, the corresponding requirement to obtain a consistent saddle-point approximation of $\mathcal{F}$ according to Eq. (20.45) will require a very large $\ell \equiv \log(1/x_B)$ compared to $L_Q = \log Q^2$. For the available ℓ-values in HERA we need such small Q^2-values that the results of perturbative QCD will no longer be valid.

It is worthwhile to further elaborate the use of a running coupling in connection with the integral equation for the non-integrated structure

https://doi.org/10.1017/9781009401296.020 Published online by Cambridge University Press

function $\mathscr{F}$ in Eq. (20.31). It turns out that the solutions are very different from the BFKL results. It is, however, not obvious how to introduce a running coupling because as mentioned above we do not know the virtual corrections to the equations at the next order of perturbation theory. There is nevertheless one feature of particular interest. A running coupling tends to diminish the κ-values along the main paths and this means in particular that the Brownian motion properties of the BFKL mechanism, i.e. that the paths can go up and down in a stochastical way in κ, is strongly disturbed. In order to understand the physics we note the difference between a stochastical motion without any constraints, i.e. when there is the same probability of going in each direction and when there is a 'force' which will make the 'particle' prefer one of the directions.

A simplified picture is given by the following model. Assume that there is a set of points x_j and assume that at time t there is a density of objects $\rho(x_j) \equiv \rho_j$ distributed over the points. The rules of the process are that during the time interval δt the objects at x_j may move either to x_{j+1} or to x_{j-1} with the probabilities $(1 \mp \alpha)/2$ respectively. For simplicity we let α be a constant between zero and one, i.e. there is a preference towards smaller j-values, which we will associate with smaller x. Then we obtain

$$\rho_j(t+\delta t) = \frac{1-\alpha}{2}\rho_{j-1}(t) + \frac{1+\alpha}{2}\rho_{j+1}(t) \tag{20.46}$$

The equation can be rewritten

$$\begin{aligned} \rho_j(t+\delta t) - \rho_j(t) &= \frac{1}{2}[\rho_{j+1}(t) - 2\rho_j(t) + \rho_{j-1}] + \frac{\alpha}{2}[\rho_{j+1}(t) - \rho_{j-1}(t)] \\ \Rightarrow \frac{\partial \rho}{\partial t} &= a\frac{\partial^2 \rho}{\partial x^2} + b\frac{\partial \rho}{\partial x} \end{aligned} \tag{20.47}$$

where b is proportional to the parameter α in the process. In the second line we have gone to the limits $x_{j+1} \to x_j$ and $\delta t \to 0$. We have consequently derived the ordinary *diffusion equation.* It is well known that when b is zero (i.e. the case of symmetry where α vanishes) then the solution, which at time zero is centred at the origin $x = 0$ as a δ-distribution, is for finite t-values given by the (normalised) gaussian distribution

$$\frac{N}{\sqrt{\pi t}} \exp\left(-\frac{x^2}{4at}\right) \tag{20.48}$$

This means that N objects, all starting at the origin, will perform a Brownian motion, i.e 'diffuse' away and after a time t on average reach the point $2\sqrt{at}$.

If b is different from zero, however, then *there are stationary, i.e. time-*

https://doi.org/10.1017/9781009401296.020 Published online by Cambridge University Press

independent, solutions of an exponential kind:

$$C \exp\left(\frac{-bx}{a}\right) \tag{20.49}$$

The distribution will settle into such a stationary state after a period which depends upon the boundary conditions. It is well known that this is just the density distribution of the atmosphere of the earth and the reason for the preference of small x-values is in that case the gravitational force.

The model described above is much too simple to describe fully the non-integrated structure function $\mathscr{F}$. It is, however, of interest that the integral equation (20.31) can under simplifying assumptions be rewritten as a second-order differential equation similar to the Schrödinger equation. Then $\mathscr{F}$ takes the role of the wave function and the coupling takes the role of a potential. In this way there will be a 'gravitational pull' towards small κ from a running coupling like $\alpha_s \propto 1/\kappa$. Unfortunately there is at present no infrared-stable solution, i.e. it is necessary to make use of some transverse momentum cutoff in the equations. Therefore we will not pursue this problem any longer.

Nevertheless, we note from the results of numerical solutions to the integral equation (20.31) that when the running-coupling solutions start to become of a BFKL kind, i.e. behave as a power in $1/x_B$, then the large-transverse-momentum tail of the distribution will exhibit an exponential falloff in κ with a slope independent of $\log(1/x_B)$. *Consequently there is no diffusion in κ leading to a gaussian distribution with a width proportional to the chain length* $\log(1/x_B)$.

In conclusion we have found that the two fundamental mechanisms, i.e. the DGLAP and the modified BFKL, are also relevant as basic analysis tools for the more complex interpolating linked dipole chain model equations ('modified BFKL' means that there is an effective λ_e essentially smaller than the original Lipatov index in Eq. (20.40)). The average paths, corresponding to the main contribution from the fan diagrams (Fig. 19.1) in the triangular phase space, are cigar-shaped when the main path is described together with the average fluctuations around it. This is nowadays known as the 'Bartel cigar', for a major contributor to the investigations. The Bartel cigar is situated along the small-κ region and contributes to the structure function behaviour in accordance with the modified BFKL mechanism. In the end the average path rises towards the required $\log Q^2$ value in accordance with the DGLAP mechanism. Owing to the limited $\log(1/x_B)$ range available, all our results inside the HERA region will be dominated by the latter mechanism.

There are, however, inside the presently available accelerator regions (referring to both the HERA and the FERMILAB facilities), the many investigations to be performed, both theoretically and experimentally,

when it comes to the transverse momentum distributions and the variations, which will go over into jets (both of the Rutherford and the ordinary bremsstrahlung kind).

Consequently the phase space for deep inelastic scattering will most certainly contain many more degrees of freedom than we know of at present!